Pre-Combustion Carbon Dioxide Capture by a New Dual Phase Ceramic-Carbonate Membrane Reactor

Final Scientific/Technical Report

Reporting Period Starting Date

October 1, 2009

Reporting Period End Date

September 30, 2014

Principal Author

Jerry Y.S. Lin

Date Report was Issued

January 31, 2015

DOE Award Number

DE-FE0000470

Submitting Organization

Arizona State University

Tempe, AZ 85287

DISCLAIMER:

Abstract

This report documents synthesis, characterization and carbon dioxide permeation and separation properties of a new group of ceramic-carbonate dual-phase membranes and results of a laboratory study on their application for water gas shift reaction with carbon dioxide separation. A series of ceramic-carbonate dual phase membranes with various oxygen ionic or mixed ionic and electronic conducting metal oxide materials in disk, tube, symmetric, and asymmetric geometric configurations was developed. These membranes, with the thickness of 10 μm to 1.5 mm, show CO_2 permeance in the range of $0.5\text{-}5\times10^{-7}$ mol m^{-2} s^{-1} Pa^{-1} in 500-900°C and measured CO_2/N_2 selectivity of up to 3000. CO_2 permeation mechanism and factors that affect CO_2 permeation through the dual-phase membranes have been identified. A reliable CO_2 permeation model was developed. A robust method was established for the optimization of the microstructures of ceramic-carbonate membranes. The ceramic-carbonate membranes exhibit high stability for high temperature CO_2 separations and water gas shift reaction.

Water gas shift reaction in the dual-phase membrane reactors was studied by both modeling and experiments. It is found that high temperature syngas water gas shift reaction in tubular ceramic-carbonate dual phase membrane reactor is feasible even without catalyst. The membrane reactor exhibits good CO_2 permeation flux, high thermal and chemical stability and high thermal shock resistance. Reaction and separation conditions in the membrane reactor to produce hydrogen of 93% purity and CO_2 stream of >95% purity, with 90% CO_2 capture have been identified. Integration of the ceramic-carbonate dual-phase membrane reactor with IGCC process for carbon dioxide capture was analyzed. A methodology was developed to identify optimum operation conditions for a membrane tube of given dimensions that would treat coal syngas with targeted performance. The calculation results show that the dual-phase membrane reactor could improve IGCC process efficiency but the cost of the membrane reactor with membranes having current CO_2 permeance is high. Further research should be directed towards improving the performance of the membranes and developing cost-effective, scalable methods for fabrication of dual-phase membranes and membrane reactors.

Table of Contents

1. Executive Summary

In this project, a series of ceramic-carbonate dual phase membranes with various oxygen ionic or mixed ionic and electronic conducting metal oxide materials (LSCF, LCGFA, BYS, YSZ and SDC) in different geometric configurations (disk, tube, symmetric, and asymmetric) were fabricated. These membranes with the thickness of 10 μm to 1.5 mm show CO_2 permeance in the range of 0.5-5×10^{-7} mol m^{-2} s^{-1} Pa^{-1} in 500-900 ^oC. The CO_2 perm-selectivity is extremely high (measured CO_2/N_2 selectivity up to 3000). Ceramic-carbonate membranes exhibited high stability for high temperature CO_2 separations. SDC-carbonate membrane can be operated stabily at high temperature and even under syngas environments for more than one month.

CO_2 permeation mechanism and factors that affect CO_2 permeation through the dual-phase membranes have been identified. CO_2 permeation flux is mainly controlled by the ionic conductivity of the ceramic phase and also affected by other factors, such as temperature, CO_2 partial pressure across the membrane, membrane thickness and membrane microstructure. A reliable CO_2 permeation model was developed. A robust method was established for the optimization of the microstructures of ceramic-carbonate membranes.

Water gas shift (WGS) reaction in the dual-phase membrane reactors was studied by both modeling and experiments. It is found that high temperature syngas WGS reaction in tubular SDC-carbonate dual phase membrane reactor is feasible even without catalyst. The membrane reactor exhibits good CO_2 permeation flux, high thermal and chemical stability and high thermal shock resistance. Modified high temperature homogeneous WGS reaction kinetic equation was developed. WGS reaction performance under wide operation conditions was predicted by the model. Conditions to produce hydrogen of 93% purity and CO_2 stream of >95% purity, with 90% CO_2 capture have been identified.

The integration of the ceramic-carbonate dual-phase membrane reactor with IGCC process for carbon dioxide capture was analyzed. By using the model, a methodology was developed to identify optimum operation conditions for a membrane tube of given dimensions that would treat coal syngas with targeted performance. The calculation results show that the dual-phase membrane reactor could improve IGCC process efficiency but the membrane reactor is too expensive with membranes having current CO_2 permeance.

2. Introduction/Background and Objective of Research

2.1 Membrane Reactors for Water-Gas-Shift Reaction

Integrated gasification combined cycle (IGCC) power generation technology includes gasification of coal, water-gas-shift (WGS) reaction to convert carbon monoxide with water to hydrogen and carbon dioxide, separation of hydrogen and CO_2 from the product stream, and removal of water vapor and other impurities (such as H_2S) from hydrogen or CO_2 stream [1]. WGS, a key step in IGCC process, is an exothermic reaction (heat of reaction: –41.1 kJ/mol), therefore thermodynamically low reaction temperatures are desired. However, high temperatures are favorable from kinetic viewpoint. Commercially WGS is conducted in two or more reactor stages with inter-cooling to maximize conversion for a given catalyst volume. In a two-stage

WGS process, the first reactor is operated at high temperatures (350-400 ^{o}C), with an iron-based catalyst of high thermal stability, and the second at comparatively low temperatures (200-250 ^{o}C) using a copper-based catalyst [2].

Removing one of the products (i.e. H_2 or CO_2) from the WGS reaction zone can break the equilibrium limitation and significantly enhance the CO conversion. Therefore, numerous studies are focused on catalytic membrane reactors for WGS reaction accompanied by the simultaneous separation of H_2 or CO_2 [3-5]. The membrane removes hydrogen (or CO_2) from the reactor, facilitating higher conversion at a given temperature. If sufficient conversion is achieved, a non-permeate stream comprising mainly CO_2 (or hydrogen) can be obtained. This arrangement represents considerable simplification of the process: using a single stage shift reactor to produce high purity hydrogen without or with only minimum additional separation/purification efforts. The envisioned application of the WGS membrane reactor is to convert CO in the coal gas from a coal gasifier to produce hydrogen rich fuel, and CO_2 rich stream which can, with minimum further treatment, be compressed for geologic sequestration.

So far, majority studies on membrane reactors for WGS reaction were conducted with hydrogen permeable inorganic membranes, in particular, metal membranes [6-8]. Lee et al. [7] developed a pilot-scale WGS reactor (1 Nm^3 h^{-1} feed gas) using Pd-Cu membranes. The CO_2 concentration of retentate flow reached 80 vol.% and the H_2 concentration of permeate flow was over 99 vol.%. Catalano et al. [8] studied the scaling up of Pd-based WGS membrane reactor with 0.02 m^2 of effective membrane area. A maximum CO conversion of 98.1% was achieved, with a H_2 recovery of 81.5% and H_2 purity of 99.97% at 440 ^{o}C and 20 bar of absolute pressure in the retentate side. Modeling of the membrane reactor for WGS reaction using mesoporous ceramic membranes (such as Vycor glass) with Knudsen separation mechanism was also reported by Damle et al. [9]. The modeling results showed that a membrane reactor made of the mesoporous membrane with low perm-selectivity for hydrogen over other gases cannot produce hydrogen and carbon dioxide streams with purities higher than 90%, though the conversion can be improved as compared to the conventional reactor.

In addition to experimental studies on WGS membrane reactors, several groups reported economic analysis on the feasibility of the membrane reactor for WGS [10,11]. Bracht et al. [10] analyzed WGS reactions on membrane reactors made of an ideal microporous silica membrane with good selectivity and high hydrogen permeance. The analysis indicates favorable investment and operational costs of the membrane reactor process. Similar conclusions on favorable investment and operation costs were also made by Criscuoli et al. [11] on a palladium membrane reactor. The practical application of the membrane reactors for WGS depends on technology for fabrication of inorganic membranes with high selectivity and permeance and low costs. A simulation study by Fluor Inc. suggests that a membrane suitable for WGS reactor application should have hydrogen permeance larger than 5×10^{-7} mol/m^2 s Pa and perm-selectivity of H_2 to CO_2 or CO higher than 50 (at 400^{o}C) [12]. In addition to selectivity, permeability and cost of a membrane, the thermal and chemical stability of the membrane is equally important for the WGS membrane reactor.

2.2 Hydrogen or CO_2 Perm-selective Inorganic Membranes

The membrane is the key component in membrane reactors for WGS. Inorganic membranes suitable for WGS membrane reactors include hydrogen or CO_2 perm-selective membranes in the gas mixture of CO, H_2O, CO_2 and H_2. Inorganic membranes with good hydrogen perm-selectivity at high temperatures are amorphous microporous carbon [13,14], amorphous silica [15,16], microporous crystalline zeolite [17, 18], - dense crystalline palladium [10,11] and perovskite type proton-conducting ceramics [19, 20]. These membranes, most prepared as thin films supported on porous ceramic or metal substrate, were studied extensively in the past two decades.

Carbon membranes show good selectivity but do not offer desired hydrogen permeance and stability. Sol-gel derived microporous silica membranes offer both good selectivity and high permeance for hydrogen. The major shortcoming for these silica membranes is their poor hydrothermal stability [21,22]. Cerate based proton-conducting ceramic membranes are hydrogen semi-permeable. However they do not offer sufficiently high hydrogen permeance in the temperature range for WGS reaction. This group of membranes are more suitable for applications at higher temperatures (>800^{o}C). Furthermore, in the gas streams containing CO and CO_2, carbonate species may form on the surface of the cerate based proton-conducting ceramic membranes, causing a substantial reduction is hydrogen permeance [23]. Crystalline palladium alloyed membranes [10,11] have extremely high hydrogen permeability and selectivity. However, the disadvantages of Pd-based membranes lie in their moderate durability and high brittleness which limit their practical applications [24,25]. Pure silica MFI type or DDR type zeolites, with a pore diameter of about 0.6 and 0.4 nm, respectively, are the most thermally and chemically stable microporous inorganic material. However, studies show that the H_2 to CO selectivity of MFI or DDR type zeolite membranes still need to be improved, because the pore size of these zeolites are too large with respect to the molecular size of hydrogen to bring about molecular sieving effect [18,26].

Besides the in-situ separation of H_2, CO_2 removal has been confirmed as another promising route to promote the WGS reaction for H_2 production. Typically, CO_2 sorbents were used for in situ CO_2 removal to enhance the reaction performance [27,28]. It is also highly desirable to use a CO_2-selective membrane for the WGS reaction because CO_2-selective membrane reactors have the potential to achieve higher H_2 recovery [29]. Moreover, CO_2 removal through the membrane retains H_2 at high pressure, maximizing the efficiency of the combustion turbine. Scholes et al. [29] also stated that if CO_2-selective WGS membrane reactors can be adapted to operate at high temperatures and pressures they will present an attractive option for the IGCC process.

About CO_2 perm-selective inorganic membranes, most studies were focused on properties of the membranes to separate CO_2 from N_2 with the intention to separate CO_2 from flue gas. Microporous inorganic membranes show perm-selective for CO_2 over N_2 due to preferential adsorption of CO_2 on the membrane material, or the smaller molecular size of CO_2 compared to N_2[30-32]. Sol-gel derived silica membranes show a CO_2/N_2 separation factor of 11 to 57 in the temperature range of 300-400^{o}C. Zeolite membranes also exhibit good separation properties at low temperatures. The maximum CO_2/N_2 separation factor is 100 at 40^{o}C for a NaY membrane. The maximum temperature studied for the separation/permeation properties is 350^{o}C for modified zirconia membranes, but the CO_2/N_2 separation factor is low (in the range of 4-6) at

this temperature. In summary, all of these inorganic membranes offer a high carbon dioxide permeance (up to about 2×10^{-6} mol/m^2 s Pa), however, their selectivity for CO_2 to N_2 diminishes as temperature increases, reaching values less than 2 at temperatures higher than 300^{o}C. No microporous or dense (single phase) inorganic membranes that exhibit a perm-selectivity for CO_2 over N_2 or H_2 at temperatures above 400^{o}C were reported in the literature. Consequently, there was a compelling need for CO_2 separation membranes that can operate under more extreme conditions while providing a high performance for sustainable CO_2 capture.

In an effort to develop CO_2 perm-selective membranes, Lin and co-workers were the first to report a metal-carbonate[33] and ceramic-carbonate[34] dual phase membrane for CO_2 separation. These dual-phase membranes have high CO_2 permeance with theoretically infinite selectivity for CO_2 over all other gases in 700-900 ^{o}C. A typical dual-phase membrane is composed of a porous ceramic phase and a molten carbonate phase (**Figure 1**). The ceramic phase serves as a porous support and also an oxygen ion (O^{2-}) conductor, while the molten carbonate phase is infiltrated into the porous support as a carbonate-ion (CO_3^{2-}) conductor. At high temperatures, CO_2 combines with O^{2-} to be CO_3^{2-} which transports through the membrane under the driving force of CO_2 partial pressure gradient.

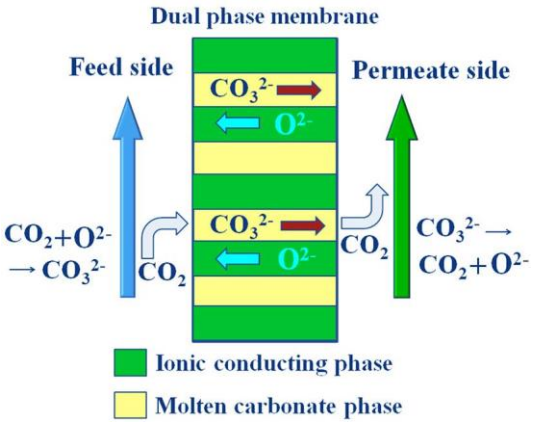

***Figure 1**: Concept of ceramic-carbonate dual phase membranes for CO_2 separation.*

2.3 Objectives of Research

This project was focused on developing a membrane reactor made of a new CO_2 semi-permeable ceramic-carbonate dual-phase membrane for syngas water gas shift (WGS) reaction for hydrogen production and carbon dioxide capture. The membrane reactor works in the similar way as the hydrogen permeable membrane for WGS, except that in the proposed membrane reactor CO_2, instead of hydrogen, is removed from the WGS reaction product stream. This will result in a low pressure CO_2 stream with purity greater than 95% in the permeate side, and high pressure, hot H_2 stream on the retentate. The objectives of this project were to (1) synthesize chemically/thermally stable dual-phase ceramic-carbonate membranes with CO_2 permeance and CO_2 selectivity (with respect to H_2, CO or H_2O) of larger than 5×10^{-7} mol/m^2 s Pa and 500; (2) fabricate tubular dual-phase membranes and membrane reactor modules suitable for WGS membrane reactor applications; and (3) identify experimental conditions for WGS in the dual-phase membrane reactor that will produce the hydrogen stream with at least 93% purity and CO_2 stream with at least 95% purity. The results obtained in this project will enable development of a large-scale one step membrane reactor process for syngas WGS reaction that will lower costs for pre-combustion carbon dioxide capture. The results obtained in this project are summarized next.

3. Results of Task A: Synthesis of Dual-Phase Membrane Disks

3.1 Properties of Molten Carbonates

In the ceramic-carbonate dual phase membrane, the molten carbonate serves as the conductor of carbonate ion. The property of carbonate is closely related to the performance of dual phase membranes. **Table 1** list carbonate ion conductivity and melting point of several carbonates. Li/Na/K mixed carbonate shows the lowest melting point and good ion conductivity. So, it was used as the carbonate phase in this project.

***Table 1**: Properties of molten carbonates.*

	Li/Na/K Carbonate	Li/K Carbonate	Li/Na Carbonate	Na/K Carbonate
Composition (mol%)	43.5/31.5/25	62/38	52/48	56/44
Melting Point (^{o} C)	397	488	501	710
CO_3^{2-} Conductivity (S/cm)	1.24	1.15	1.75	1.17

3.2 Oxygen Ion Conducting Ceramic Supports

In the ceramic-carbonate dual phase membrane, the oxygen ion conducting ceramic support is used not only for the transport of oxygen ion but also for holding the molten carbonate. The property of oxygen ion conducting material and the support significantly affect the performance of the dual phase membrane. The basic requirements for the oxygen ion conducting material and support are: 1) high ionic conductivity; 2) long-term chemical stability; 3) compatible with molten carbonate; 4) controllable pore size, porosity. In this project, five different oxygen ionic (or mixed ionic and electronic) conducting materials were used as the ceramic support of dual phase membranes (**Table 2**). Some materials show high stability but with relatively low oxygen ion conductivity, such as LCGFA. Some of them show high oxygen ion conductivity, however they are easy to react with CO_2, such as LSCF. In contrast, SDC shows both high oxygen ion conductivity and stability, and is a promising ceramic material for dual phase membranes.

***Table 2**: Properties of oxygen ionic (or mixed) conducting ceramic materials.*

Material	Abbreviation	Structure	O^{2-} conductivity σ_i (600 ^{o}C) (S/cm)	Transference number t_i
$La_{0.85}Ce_{0.1}Ga_{0.3}Fe_{0.65}Al_{0.05}O_{3-\delta}$	LCGFA	Perovskite	~ 0.001	~ 0.02
$La_{0.6}Sr_{0.4}Co_{0.8}Fe_{0.2}O_{3-\delta}$	LSCF	Perovskite	~ 0.003	~ 0.01
8mol% Y_2O_3 stabilized ZrO_2	YSZ	Fluorite	~ 0.004	~ 1.0
$Sm_{0.2}Ce_{0.8}O_{2-\delta}$	SDC	Fluorite	~ 0.005	~ 1.0
$Bi_{1.5}Y_{0.3}Sm_{0.2}O_{3-\delta}$	BYS	Fluorite	~ 0.08	~ 0.9

3.3 Synthesis of Ceramic-Carbonate Disk Membranes

Ceramic powders were synthesized via the citrate method from the metal nitrates[35]. Take SDC for example, stoichiometric amounts of $Ce(NO_3)_3$ $6H_2O$ (Alpha Aesar) and $Sm(NO_3)_3$ $6H_2O$ (Alpha Aesar) were mixed into a measured volume of deionized water under continuous agitation, followed by the addition of citric acid (mole ratio of total metal ions to citrate is 1:2) with stirring. The solution containing the complex precursor was then heated on a hot plate to 250-400 ^oC. Upon heating, the solution boiled and formed a gel. The gel underwent a dehydration and decomposition process and produced a foam-like solid, which ignited to produce a soft and fluffy product. Finally, the products were calcined in air at 550 ◦C for 8 h to prepare SDC oxide. Other powders were prepared by the same method. After self-ignition, the oxides were synthesized after the calcination at 900 ^oC for 5h.

For the preparation of ceramic disks, ceramic powders were mixed with small amount of 3wt% PVA. Approximately 3g of powder was placed in a 30mm stainless steel mold and pressed to 160 MPa for 5min using a hydraulic press. The green disks were then sintered at 900-1100 ^oC (depends on materials) for about 20h with heating and cooling ramping rates of 2 ^oC/min, resulting in porous ceramic disk supports.

Synthesis of ceramic-carbonate dual-phase membranes was achieved by direct infiltration of molten carbonate into the pores of sintered ceramic supports via the direct infiltration technique [33]. The carbonate powders Li_2CO_3 (99.2%, Fischer Scientific), Na_2CO_3 (99.9%, Fischer Scientific), and K_2CO_3 (99.8%, Fischer Scientific) were weighed out in a 42.5/32.5/25 mol% ratio, respectively, and heated to 550 ^oC in a furnace (**Figure 2**). Porous ceramic supports were preheated above the molten carbonate mixture to prevent thermal shock prior to being lowered into contact with carbonate. Supports were left in contact with molten carbonate for 5–10 min to ensure complete infiltration via capillary force. The membrane was then lifted and slowly removed from the furnace and cooled. Residual carbonate on the membrane surface was removed using a SiC polishing paper.

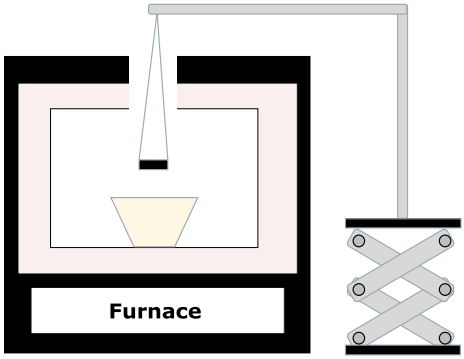

***Figure 2**: Schematic of the carbonate infiltration process.*

3.4 Characterization of Ceramic-Carbonate Dual Phase Membranes

For porous ceramic supports and ceramic-carbonate membranes, the morphology, crystal structure, and gas permeation performance behaviors were analyzed. Take LSCF-carbonate dual phase membrane as example, the morphology is shown in **Figure 3**. LSCF support is porous, while the dual phase membrane is dense after infiltration with carbonate. The LSCF phase is combined well with the carbonate phase. The LSCF support shows typical perovskite structure (**Figure 4**). In contrast, the LSCF-carbonate dual-phase membrane exhibits both perovskite phase and carbonate phase (from 24^o to 30^o). The gas permeation analysis shows that the He permeance of the LSCF support is ~10^{-6} mol/m^2 s Ꝑa. After infiltration with carbonate, the weight of the support increases 25%, and the He permeance is lower than 10^{-10} mol/m^2 s Ꝑa.

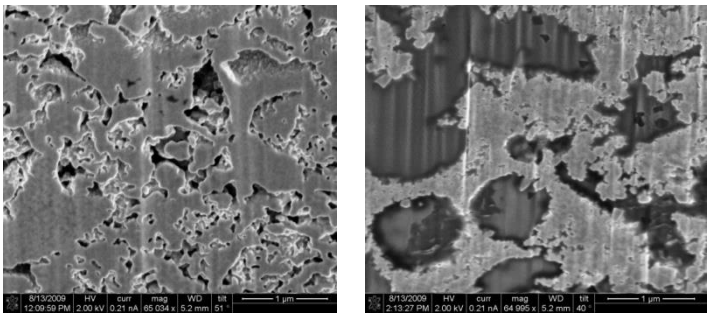

***Figure 3**: SEM images of LSCF porous support (left) and LSCF-carbonate dual phase membrane (right).*

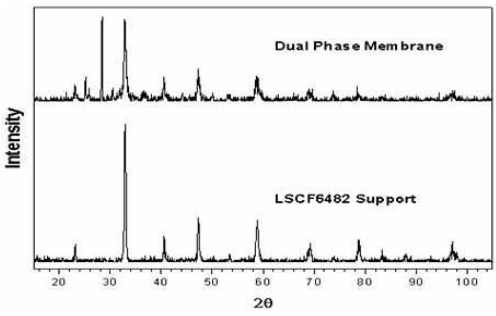

***Figure 4**: XRD patterns of LSCF porous support and LSCF-carbonate dual phase membrane*

3.5 Thin Ceramic-Carbonate Dual Phase Membranes

To increase CO_2 permeance of ceramic-carbonate dual phase membranes, we proposed to synthesize an asymmetric ceramic-carbonate membrane with a thin dense membrane layer supported by a porous support, as shown in **Figure 5**. The asymmetric support should consist of a thick (1–2 mm), large pore (0.5–5 μm) base and a thin (5–50 μm), small pore (~100 nm), oxygen ionic conducting or mixed conducting ceramic top-layer. The molten carbonate fills in the pores of the top-layer by a direct infiltration. The key point is to ensure that after infiltration with carbonate the top-layer is gas tight while the base remains porous. To realize this purpose, a carbonate un-wetable material BYS was selected to prepare the macroporous base. YSZ and SDC were used to prepare the top layers, respectively. YSZ/BYS asymmetric support was prepared by a dip-coating method [36], while SDC/BYS-SDC asymmetric support was prepared by a co-press method [37].

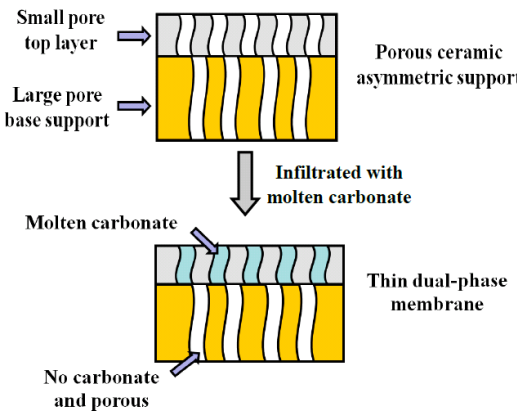

***Figure 5**: Schematic configuration of asymmetric thin dual-phase membrane.*

The morphologies of YSZ/BYS and SDC/BYS-SDC asymmetric supports and membranes are shown in **Figure 6**. From **Figures 6a-6c**, the YSZ top layer prepared by dip-coating is continuous and defect-free. The particle size of YSZ is about 200 nm. The YSZ layer with the thickness of 10 μm is bonded well with the BYS support. After infiltration the YSZ layer becomes dense. From **Figures 6d-6f**, before infiltration, the SDC top layer is porous with the pore size of about 1-2 μm and particle size of about 1 μm. The SDC top layer prepared by co-pressing method is bound well with the BYS-SDC support. The thickness of SDC layer is about 150 μm. After infiltration the SDC top layer becomes dense and it shows 2 to 3 orders of magnitude drop in helium permeance.

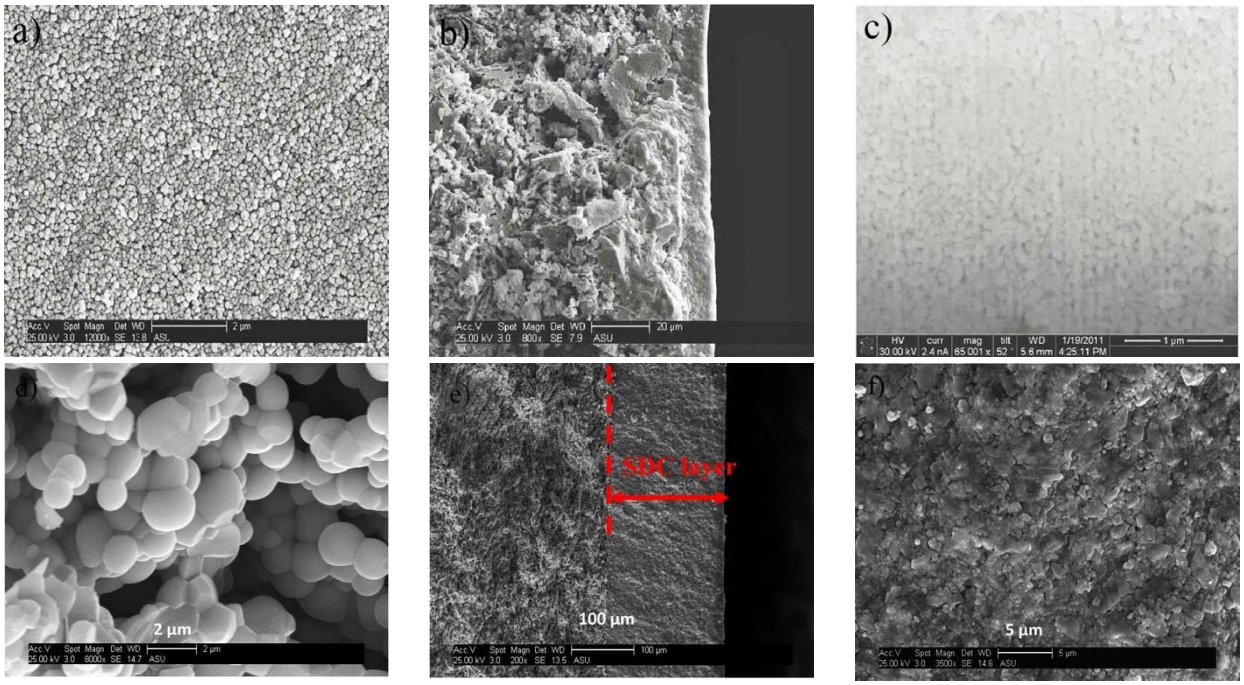

Figure 6*: SEM images of YSZ/BYS: (a) surface of porous YSZ top layer; (b) cross-section of YSZ/BYS membrane; (c) surface of YSZ top layer after infiltration; and SDC/BYS-SDC: (d) surface of porous SDC top layer; (e) cross-section of SDC/BYS-SDC membrane; (f) cross-section of SDC top layer after infiltration.*

4. Results of Task B: Studying Permeation and Separation Properties of Disk Membranes

4.1 Gas Permeation Measurement Setups

In this project, two types of gas permeation setups were developed for the CO_2 permeation analysis at high temperature. One is the ceramic-tube setup, as shown in **Figure 7**. The membrane is placed at one side of a dense alumina tube and sealed by a silver ring or glass sealant. This setup can be used to test the CO_2 permeation performance up to 950 ^oC and under atmospheric pressure at both feed and permeate sides. Another is the stainless steel setup, as shown in **Figure 8**. The membrane is sealed by two graphite gaskets and placed in a stainless steel module. This setup can be used for CO_2 permeation analysis up to 700 ^oC and under both atmospheric and high feed pressures.

4.2 CO_2 Separation Performance

The CO_2 separation performance of thin YSZ [36], modified BYS [38], thick LSCF [34], LCGFA [39] and SDC [40] membranes were tested at the temperature of 500-900 ^oC. The CO_2 concentration at the feed side was 50% (25% for YSZ thin membrane). Both feed (CO_2 and N_2) and sweep (He) flow rates were 100 mL min^{-1}. The CO_2 permeation fluxes are shown in **Figure 9**. CO_2 flux increases with increasing the temperature, especially for the thick SDC membrane. CO_2 flux of thick SDC membrane increases from 0.16 mL cm^{-2} min^{-1} at 700 ^oC to 0.68 mL cm^{-}

^{2} min^{-1} at 900 ^{o}C. Reduction of the thickness of membrane layer can greatly improve the CO_2 flux. Thin YSZ membrane shows good CO_2 flux (0.26 mL cm^{-2} min^{-1}) even at relatively low temperature (650 ^{o}C). For all membranes, CO_2/N_2 selectivities are in the range of 200-3000. **Table 3** summarizes CO_2 permeation characteristics of these five dual-phase membranes.

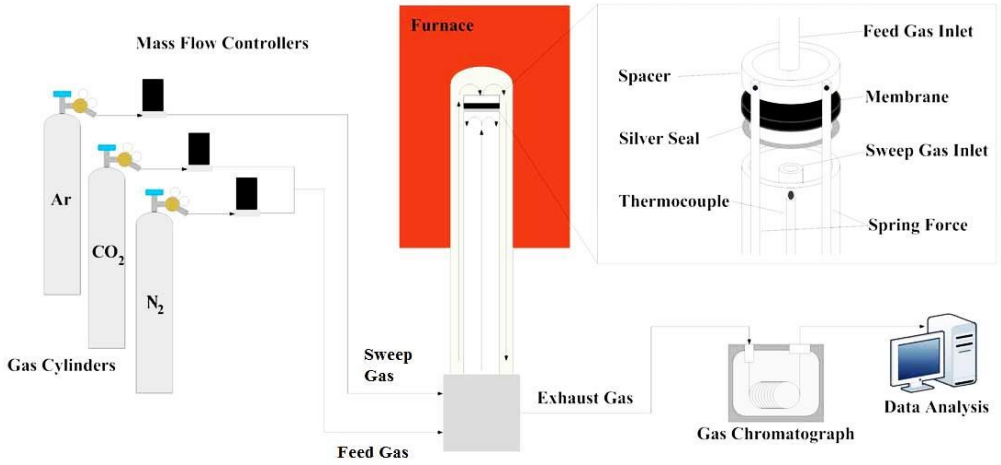

***Figure 7**: Schematic of ceramic setup for CO_2 separation test.*

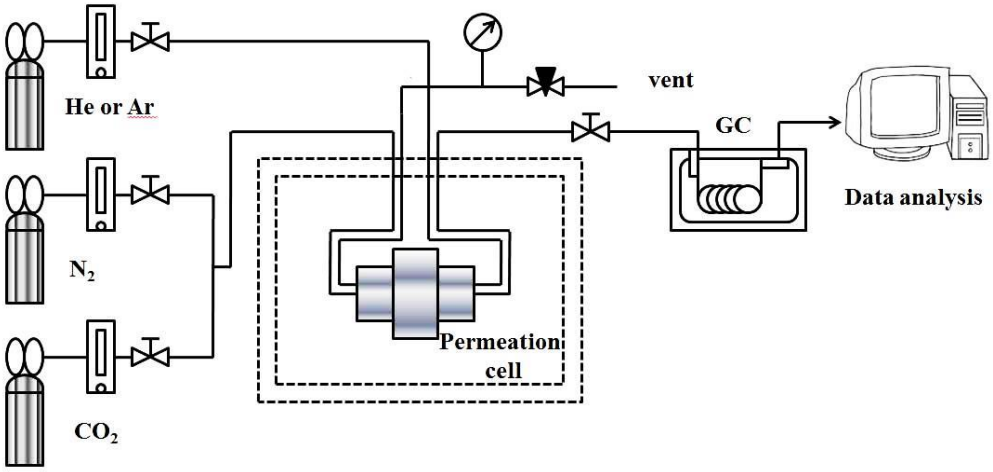

***Figure 8**: Schematic of stainless steel setup for CO_2 separation test.*

From **Figure 9**, the CO_2 permeation process through the membrane is closely related to the transportation of CO_3^{2-} and O^{2-}. Considering that all of the membranes contain the same carbonate phase, the main differences between CO_2 fluxes may be caused by the different oxygen ion transport rate. Therefore, the ionic conductivity of SDC, LSCF and LCGFA were tested, as shown in **Figure 10**. For comparison, the ionic conductivity of molten carbonate was provided. The CO_3^{2-} conductivity in molten carbonate is much higher than the O^{2-} conductivity in SDC, LSCF and LCGFA. Therefore, the CO_2 permeation flux is mainly controlled by oxygen ionic conductivity of ceramic phases. The oxygen ionic conductivity decreases in the order of SDC> LSCF> LCGFA. This trend is consistent with the CO_2 flux in **Figure 9**.

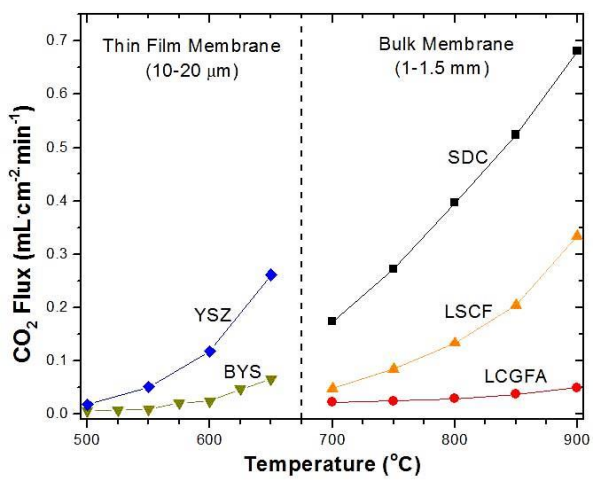

***Figure 9**: CO_2 flux of various membranes.*

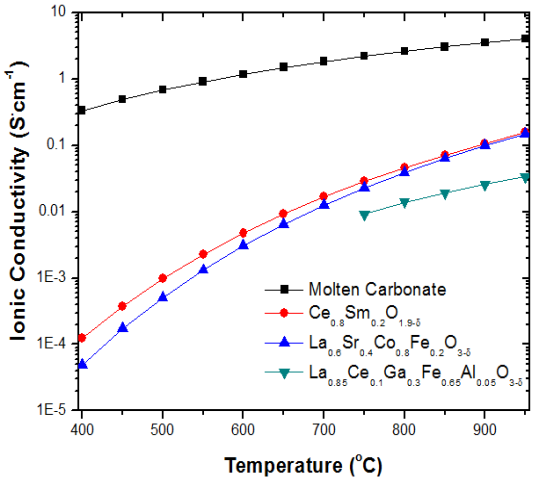

***Figure 10**: Ionic conductivity of various materials.*

***Table 3**: Summary of CO2 permeation properties of five*

Material	Abbreviation	Membrane thickness (μm)	Typical CO_2 Permeation flux		Activation energy for permeation (kJ/mol)
			Temp (^oC)	Flux# (cc/min.cm^2)	
$La_{0.85}Ce_{0.1}Ga_{0.3}Fe_{0.65}Al_{0.05}O_{3-\delta}$	LCGFA	1500	900	0.33	88
$La_{0.6}Sr_{0.4}Co_{0.8}Fe_{0.2}O_{3-\delta}$	LSCF	1500	900	0.032	97
$Sm_{0.2}Ce_{0.8}O_{2-\delta}$	SDC	1500	900	0.68	63
$Bi_{1.5}Y_{0.3}Sm_{0.2}O_{3-\delta}$	BYS	50	650	0.07	113
8mol% Y_2O_3 stabilized ZrO_2	YSZ	10	650	0.28	106

 # P'_{CO2}=0.5 atm, He as sweep gas, at total pressure of 1 atm in the feed and sweep.

Figure 11 shows the CO_2 permeation flux of thin (150 μm) SDC-carbonate membrane [37]. CO_2 flux increases from 1.33×10^{-3} to 6.55×10^{-3} mol m^{-2} s^{-1} (about 0.88 mL cm^{-2} min^{-1}) when the temperature changes from 550 to 700 ℃. At 700℃ the CO_2 flux of thin SDC-carbonate membrane is 5.5 times of the thick membrane. The thin membrane exhibits a stable CO_2 flux about 6.55×10^{-3} mol m^{-2} s^{-1} for 160 h. The test was discontinued due to system leakage from decomposition of graphite seals above 650 ℃. Longer stability is expected with the proper sealing materials.

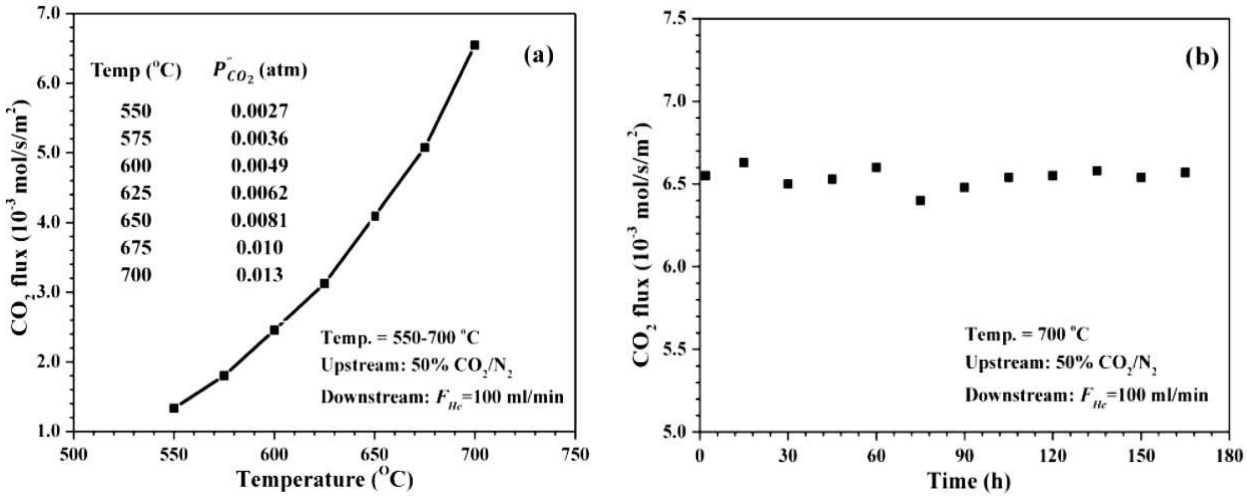

***Figure 11**: CO_2 permeation flux of thin SDC-carbonate membrane on SDC-BYS support as a function of (a) temperature and (b) permeation time.*

4.3 Effects of Microstructures of the Support and Thickness of Membranes on CO_2 Permeation

The microstructures of ceramic supports show significant effects on the CO_2 permeation performance of the ceramic-carbonate membranes. CO_2 permeance in the dual-phase membrane can be described by [41]:

$$F_{CO_2} = \frac{\alpha_s RT}{4F^2 L\left(P'_{CO_2} - P''_{CO_2}\right)} ln\left(\frac{P''_{CO_2}}{P'_{CO_2}}\right) \qquad (1)$$

where the total conductance α_s can be expressed as:

$$\alpha_s = \frac{\left(\frac{\varepsilon}{\tau}\right)_p \sigma_c \left(\frac{\varepsilon}{\tau}\right)_s \sigma_i}{\left(\frac{\varepsilon}{\tau}\right)_p \sigma_c + \left(\frac{\varepsilon}{\tau}\right)_s \sigma_i} \qquad (2)$$

and ε and τ are porosity and tortuosity, the subscript *p* and *s* refer to pore and solid (ceramic), and the σ_c and σ_i are conductivities of carbonate ion in carbonate and oxygen ion in ceramic, respectively.

To achieve highest permeance for a given dual-phase membrane with specific carbonate and ceramic materials and membrane thickness, Eq. (2) should be maximized. In this project, take LSCF-carbonate dual phase membrane for example, the microstructure of LSCF support was optimized to produce maximum total conductance (α_s) [42]. LSCF supports with different microstructures were prepared by sintering at different temperatures. σ_i and σ_c are tested at a given temperature (**Figure 10**). The porosity to tortuosity ratio of the carbonate phase $(\varepsilon/\tau)_p$ is estimated by calculations using unsteady-state helium permeation of the porous ceramic supports:

$$\left(\frac{\varepsilon}{\tau}\right)_{Pore} = \left(\frac{\alpha^2}{\beta}\right)\left(\frac{M_w L}{8.988\mu}\right) \qquad (3)$$

where L is the membrane thickness, μ and M_w are viscosity and molecular weight of permeating

gas. The values of α and β can be regressed according to the intercept and slope, respectively, in Eq. (4).

$$F=\alpha+\beta P_{avg} \quad (4)$$

where F is the gas permeance of the LSCF porous support, P_{avg} the average pressure across the LSCF support. The He permeance of different LSCF supports as a function of average pressure across the support is shown in **Figure 12**. The porosity to tortuosity ratio of the ceramic support $(\varepsilon/\tau)_s$ is estimated by measuring the conductivity of the porous ceramic support relative to dense ceramic support of the same material:

$$\left(\frac{\varepsilon}{\tau}\right)_{Solid}=\left(\frac{\sigma_s}{\sigma_i}\right) \quad (5)$$

where σ_s is the ionic conductivity of the porous ceramic support. The ionic conductivity of dense and porous LSCF and the estimated $(\varepsilon/\tau)_s$ are shown in **Figure 13**. According to Eq. (3), the total conductance (α_s) of LSCF supports sintered at different temperature can be estimated, and the results are shown in **Figure 14**. The total conductance increases and, after reaching a maximum, decreases with increasing sintering temperature. This is because the solid fraction to tortuosity ratio increases with increasing sintering temperature, but the carbonate fraction to tortuosity factor in general decreases with increasing sintering temperature. Thus, there is an optimum sintering temperature that would give a support with maximum total conductance.

Figure 14 also plots CO_2 permeance at 900 ^oC as a function of sintering temperature of the LSCF supports. As shown, the permeance also increases, and after reaching a maximum, decreases with increasing sintering temperature. Such dependence of CO_2 permeance on sintering temperature of the support is also found for CO_2 permeance measured at other permeation temperatures. Since the support porosity decreases with increasing sintering temperature, the results show that there is an optimum porosity (or sintering temperature) for the support that results in the highest CO_2 permeance.

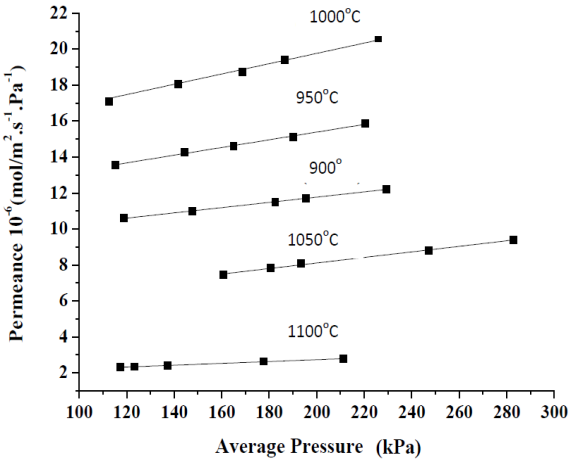

***Figure 12**: Helium permeance versus average pressure for porous LSCF supports prepared at different sintering temperatures.*

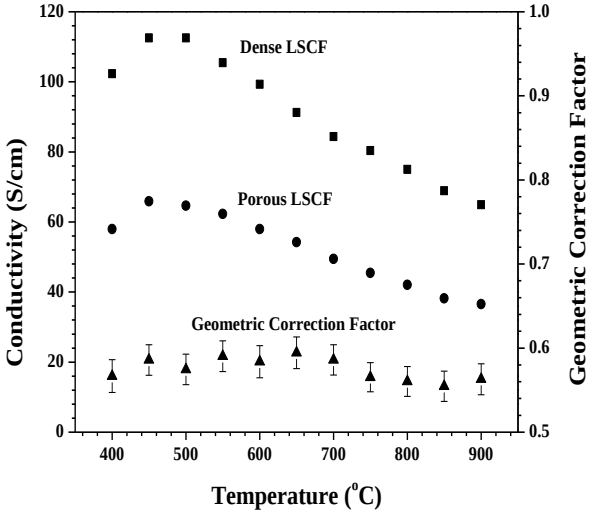

***Figure 13**: Electrical conductivity of porous and dense LSCF ceramic for solid phase structure.*

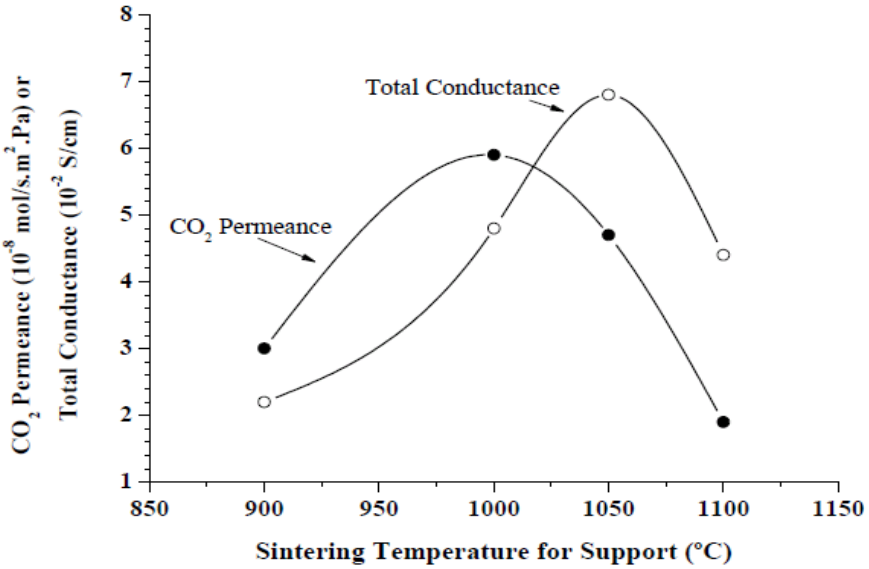

***Figure 14**: Correlation of CO_2 permeance of the dual-phase membranes with total conductance.*

However, the optimum sintering temperature to produce the maximum total conductance does not match with the optimum temperature to provide the maximum CO_2 permeance. The possible reasons are: (1) $(\varepsilon/\tau)_{pore}$ obtained from helium permeation (for gas) may not be exactly the same as $(\varepsilon/\tau)_c$ for carbonate ion transport; (2) carbonate conductivity data and LSCF oxygen ionic conductivity data from the separate phases may not be exactly the same as those phases when present in the dual-phase membrane system, and (3) using the term $(\varepsilon/\tau)_s$ to describe the oxygen conduction in the oxide phase ignores possible contributions of oxygen ions through grain boundaries. Nevertheless, the calculation results semi-quantitatively explain the experimentally observed permeance data for dual-phase membranes with supports of different structures.

Based on these results, the microstructure of disk SDC support was also optimized. The results show that the green disk SDC support with 15 wt% graphite and sintered at 1350 ^oC exhibits optimized structure. The CO_2 permeation performance of this disk SDC-carbonate membrane is shown in **Figure 15**. Under certain conditions, the CO_2 permeance of this membrane is higher than the targeted (milestone) 5×10^{-7} $mol{\cdot}m^{-2}{\cdot}s^{-1}{\cdot}Pa^{-1}$.

The effect of the membrane thickness on CO_2 permeation can be found by examining the CO_2 permeation flux data for thick (2 mm) and thin (150 μm) SDC-carbonate membranes shown in **Figures 9** and **11**. At 700^oC the CO_2 permeation flux thin SDC-carbonate membrane is about 0.88 mL cm^{-2} min^{-1}, 5.5 times larger than that for the thick SDC-carbonate membrane. Reducing membrane thickness is effective in improving CO_2 permeation flux. However, the increase in the CO_2 permeation flux is not proposal to the reduction in membrane thickness. This indicates that the surface reaction rate plays a role in controlling CO2 permeation through the dual-phase membranes studied.

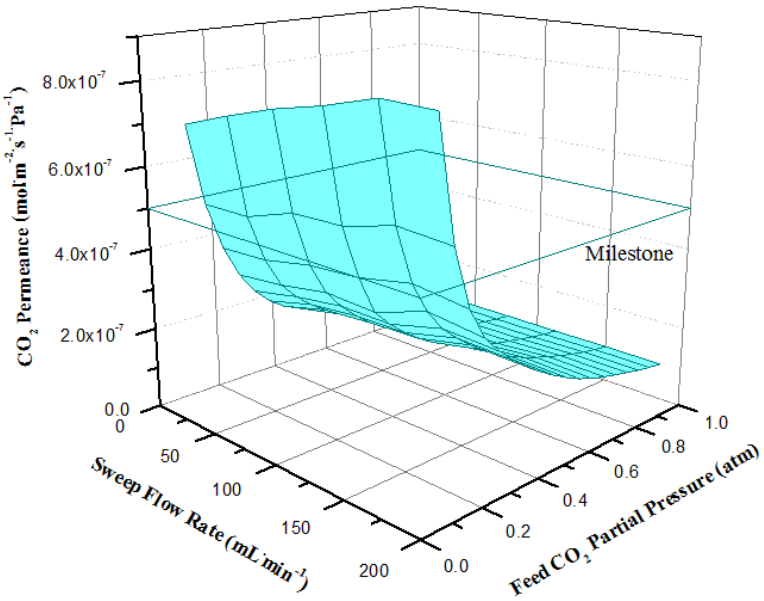

Figure 15: *Measured CO_2 permeance of SDC-carbonate dual-phase membrane at 900°C with various sweep flow rates and feed CO_2 partial pressures. Results are shown in comparison to the targeted CO_2 permeance of 5×10^{-7} $mol{\cdot}m^{-2}{\cdot}s^{-1}{\cdot}Pa^{-1}$.*

4.4 Effects of CO_2 Pressures on CO_2 Permeation

The flux equation for CO_2 permeation through ceramic-carbonate membranes at high temperature was developed as [41]:

$$J_{CO_2} = \int_{P''_{CO_2}}^{P'_{CO_2}} \alpha_s \cdot \frac{RT}{4F^2L} \cdot dLn(P_{CO_2}) \qquad (6)$$

where α_s is a permeance coefficient (or referred to as total conductance) defined as Eq. (2). R is the ideal gas constant, T is the system temperature, F is Faraday's constant, L is the membrane thickness, P'_{CO2} and P''_{CO2} are the feed and sweep sides CO_2 partial pressures, respectively, ε and τ denote the porosity and tortuosity of either the molten carbonate phase (p or c) or the solid ceramic phase (s). Under most conditions, $\sigma_c >> \sigma_i$, then $\alpha_s \sim [(\varepsilon/\tau)_s\ \sigma_i]$ and the total conductance is equal to the effective oxygen ionic conductivity of the ceramic metal oxide phase. Assuming α_s is independent of P_{CO2}, integration of Eq.(6) gives to Eq.(7).

$$J_{CO_2} = \alpha_s \cdot \frac{RT}{4F^2L} \cdot Ln\left(\frac{P'_{CO_2}}{P''_{CO_2}}\right) \qquad (7)$$

According to the experimental data of a disk SDC-carbonate membrane at 700 °C, the plot of J_{CO2} versus $\ln(P'_{CO2}/P''_{CO2})$ gives a straight line (**Figure 16**). However, it can be found that this straight line deviates far from the origin of the J_{CO2} versus $\ln(P'_{CO2}/P''_{CO2})$ coordinate, suggesting that Eq.(7) does not describe pressure dependence of CO_2 permeation flux for the ceramic-carbonate membranes. Therefore, this equation is not valid to describe CO_2 pressure dependence of CO_2 permeation flux.

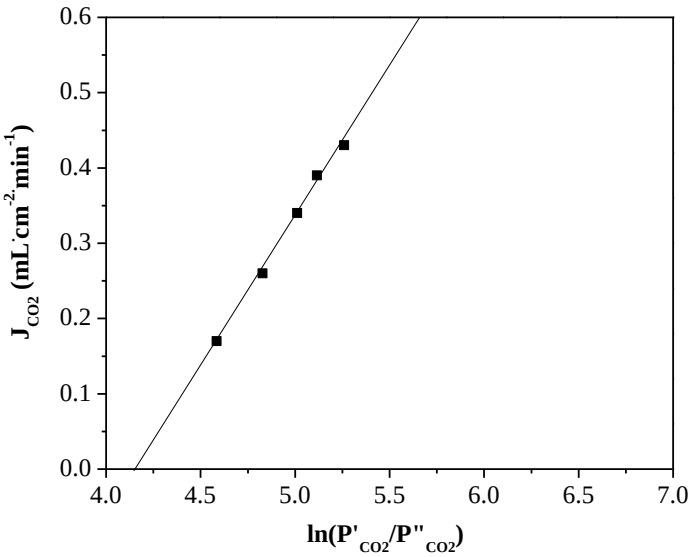

***Figure 16**: Plots of CO_2 permeation flux versus logarithmic CO_2 pressure ratio for disk SDC-carbonate membrane under high pressure CO_2:N_2 feed at 700 ^oC.*

Oxygen ionic conductivity of an ionic or mixed-conducting ceramic is known to depend on oxygen partial pressure and the dependence can be approximated by a power function [43,44]. Assuming such power function also applies to the total conductance (α_s), then

$$\alpha_s = \alpha_{so} P_{O_2}^m \qquad (8)$$

where α_{so} is the total conductance at 1 atm oxygen pressure and m is a constant which may depend on temperature. The oxygen partial pressure can be correlated to CO_2 partial pressure by either a mass balance on impurity oxygen in CO_2 and N_2 feeds for the CO_2:N_2 mixture or a thermodynamic equilibrium relation for the reaction CO_2=CO+1/2O_2. The relationship can be approximated by:

$$P_{O_2} = \varphi P_{CO_2}^q \qquad (9)$$

where φ and q are constants for Eq.(9). Inserting Eqs.(8) and (9) into Eq.(6) and integrating with respect to P_{O2}, and then changing P_{O2} to P_{CO2} using Eq.(9) yields Eq.(10).

$$J_{CO_2} = \alpha_s{}' \cdot \frac{RT}{4F^2L} \cdot (P'_{CO_2}{}^n - P''_{CO_2}{}^n) \qquad (10)$$

In Eq.(10), n=mq, and α_s' is modified total conductance at 1 atm oxygen partial pressure, i.e., $\alpha_s' = \alpha_{so}\varphi^m/n$. Eq. (10) can be further simplified to be Eq. (11) because α_s' can be expressed using Arrhenius equation and other parameters are all constant except T.

$$J_{CO_2} = A \cdot Exp\left(-\frac{Ea}{RT}\right) \cdot T \cdot (P'_{CO_2}{}^n - P''_{CO_2}{}^n) \qquad (11)$$

The parameters (pre-exponential factor A, the activation energy for oxygen ion conduction, Ea, and the pressure exponent n) in Eq. (11) were obtained by fitting the equation with the experimental data.

According to the CO_2 permeation flux data in **Figure 16**, the plot of plot J_{CO2} versus $P'_{CO2}{}^n$-$P''_{CO2}{}^n$ is given in in **Figure 17**, and as shown, it exhibit a straight line going through the origin of the coordinate, confirming that Eq.(11) weel describes the CO_2 pressure dependence of the CO_2 permeation flux through the SDC-carbonate membrane. The value of pressure exponent n is fitted to be 0.5 for flux versus CO_2 pressure data at 700 ^{o}C [40].

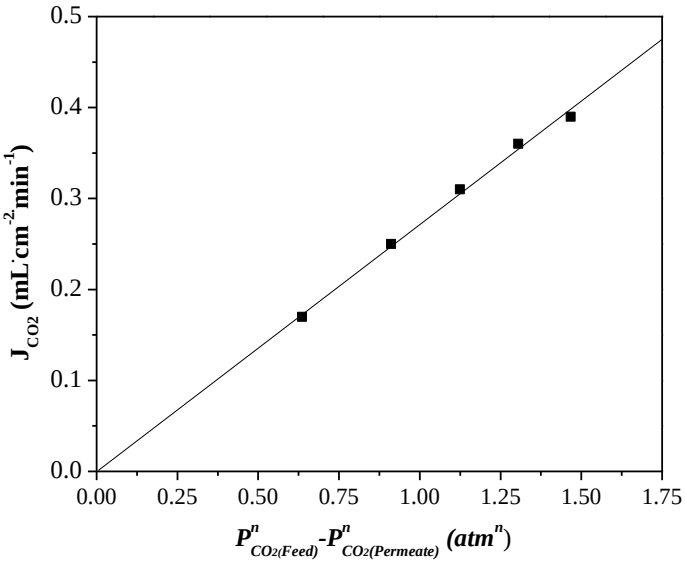

***Figure 17**: Effect of CO_2 partial pressure gradient with power function fit on CO_2 permeation flux of disk SDC-carbonate membranes with high pressure CO_2:N_2 feed at 700 ^oC.*

To further confirm the reliability of the pressure exponent n= 0.5, the data of CO_2 permeation flux of a SDC-carbonate dual-phase membrane measured at 900 ^oC was analyzed according to Eq. (11). As shown in **Figure 18**, the pressure exponent n is well fitted to be 0.5.

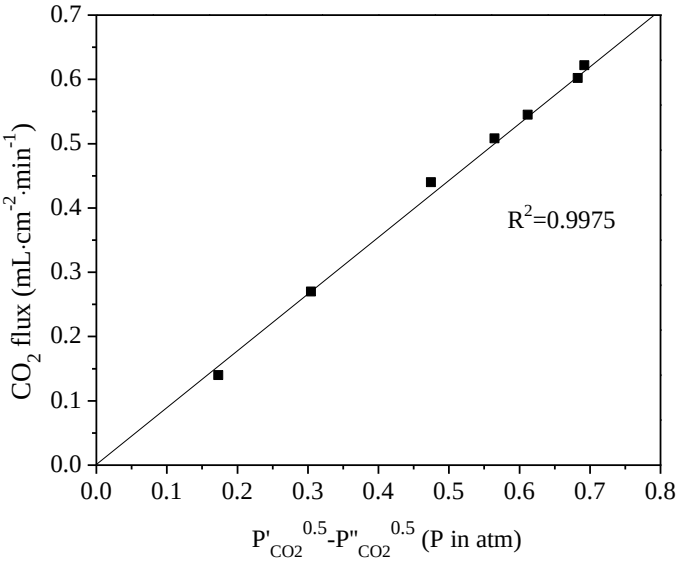

***Figure 18**: Effect of CO_2 partial pressure gradient with power function fit on CO_2 permeation flux of SDC-carbonate membrane with atmospheric CO_2:N_2 feed 900 ^oC.*

The reliability of Eq. (11) was also confirmed by the CO_2 permeation flux of a thin SDC-carbonate dual-phase membrane (150 μm) measured at 700 ^oC [37]. As shown in **Figure 19**, the pressure exponent n is well fitted to be 0.5.

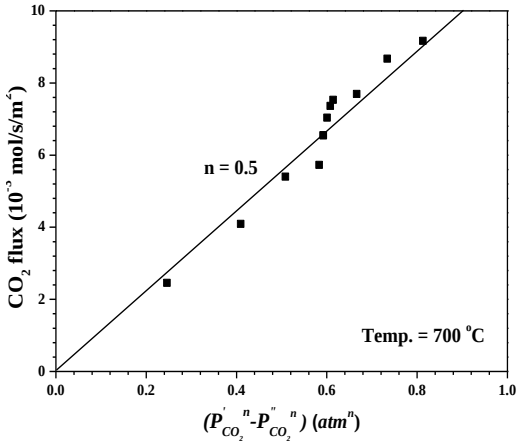

***Figure 19**: CO_2 permeation flux through thin SDC-carbonate dual phase membrane versus $P'_{CO2}{}^{n}$-$P''_{CO2}{}^{n}$.*

5. Results of Task C: Synthesis of Tubular Dual-Phase Membranes

5.1 Preparation of Tubular SDC-Carbonate Dual Phase Membranes

SDC tubular support was prepared using a centrifugal casting method. About 50 wt% SDC, 50wt% water and a few drops of PVA solution were mixed and ball milled at 175 rpm for 2h to prepare homogeneous SDC slurry. The SDC slurry was poured into the stainless steel mould with an inner diameter of 1.2-1.3 cm. After centrifugation on a homemade machine for 20 min at the spin rate of 4000 rpm, the green tubes were dried in a humidity chamber at 40 ^{o}C with a relative humidity of 60% for 12 h. Then, the green tubes were sintered at 1420 ℃ for 12h. The thickness of the SDC tube could be controlled by the amount of the added SDC slurry. SDC tubular supports with a thickness of 1.5 mm were prepared.

SDC-carbonate dual-phase membranes were obtained via a direct infiltration of molten carbonates into the SDC supports. Lithium (Li), sodium (Na), and potassium (K) carbonates from Alpha Aesar (Li_2CO_3, 99.2%; Na_2CO_3, 99.9%; K_2CO_3, 99.8%) were mixed in the mole ratio of 42.5%: 32.5%: 25% and heated to 600 ^{o}C in a box furnace. The porous SDC supports were preheated in the furnace, then vertically dipped into the molten carbonate and held for 1h. After removing the excess carbonate on the inner and outer surface, the dual-phase membranes were obtained.

Morphologies of SDC tubular supports and SDC-carbonate dual phase membranes are shown in **Figure 20**. SDC tubular supports with various sizes can be prepared by different molds. SDC supports are porous with the porosity of about 35-40% (**Figures 20b** and **20c**). After infiltration with molten carbonates, the dense SDC-carbonate membranes with clear dual-phase structure were formed (**Figures 20d-20f**).

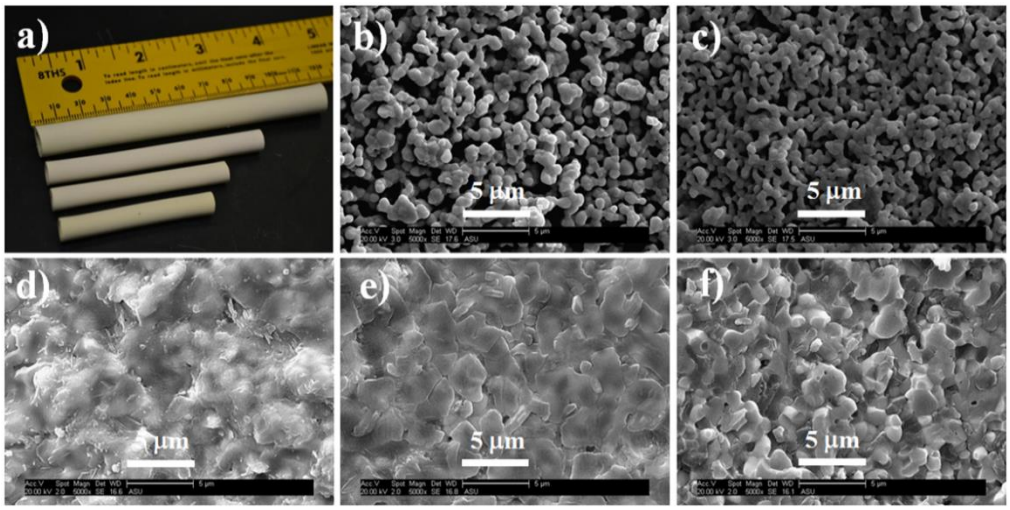

Figure 20: *(a) Photo of SDC substrates with different sizes; SEM images: (b) outer and (c) inner surfaces of SDC substrate sintered at 1420 ℃ for 12h; (d) outer and (e) inner surfaces of SDC-carbonate membrane after infiltration; (f) cross section of SDC-carbonate membrane.*

5.2 Preparation of Tubular Asymmetric SDC-Carbonate Dual Phase Membranes

To further improve the CO_2 permeation performance, the preparation of tubular asymmetric SDC-carbonate dual phase membrane was proposed. The SDC/SDC-BYS tubular support was prepared using the centrifugal casting method and underwent similar processes as the preparation of symmetric supports [45]. 55 wt% SDC (calcined at 900 ^{o}C) and 45 wt% BYS powders were mixed with water (the powder to water ratio was about 50wt%:50wt%). A few drops of 3wt% PVA solution were added into the mixture. This mixture was ball milled at 175 rpm for 3h to prepare the SDC-BYS slurry. In addition, dilute SDC slurry was also prepared via the ball mill method using 98wt % 550 ^{o}C calcined SDC and 2 wt% graphite powders, and the powder to water ratio was about 15wt%:85wt%. As shown in **Figure 21**, homogeneous SDC-BYS suspension was poured into the stainless steel mold. After centrifugation for 20 min at the rate of 4200 rpm, the liquid in the middle of the tube was poured out and the dilute SDC slurry was added. After the second centrifugation for 20 min at the rate of 4200 rpm, green tube was dried at 40 ^{o}C for 12 h. The asymmetric tube with a thin SDC inner layer and a thick SDC-BYS outer layer was obtained after sintering at 1120 ^{o}C for 12h.

The crystal structures of the porous SDC-BYS support and dense SDC-carbonate membrane layer were analyzed to confirm the chemical compatibility of SDC, BYS and carbonate. As shown in **Figures 22a** and **22b**, the SDC and BYS exhibit typical fluorite structure. From **Figures 22c**, both SDC and BYS phase are observed in the porous support, indicating that SDC is chemically compatible with BYS. **Figures 22d** exhibits mixed crystal phases of SDC and carbonate. Two carbonate diffraction peaks can be found from 20 to 25 degrees. No obvious impurity phase can be observed, suggesting that SDC and BYS are chemically compatible with carbonate.

The morphologies of asymmetric SDC/SDC-BYS tubular supports and SDC/SDC-BYS-carbonate dual phase membranes are shown in **Figure 23**. Porous SDC thin layer with the

thickness of about 120 μm is well bound with the thick SDC-BYS porous layer. The porous size of SDC-BYS layer is homogeneous and much bigger than that of the SDC layer, resulting in the low gas transporting resistance. After infiltration the SDC layer becomes dense. The SDC and carbonate phases are combined well with each other. Because of the un-wettablity of BYS, the SDC-BYS layer remains porous after infiltration.

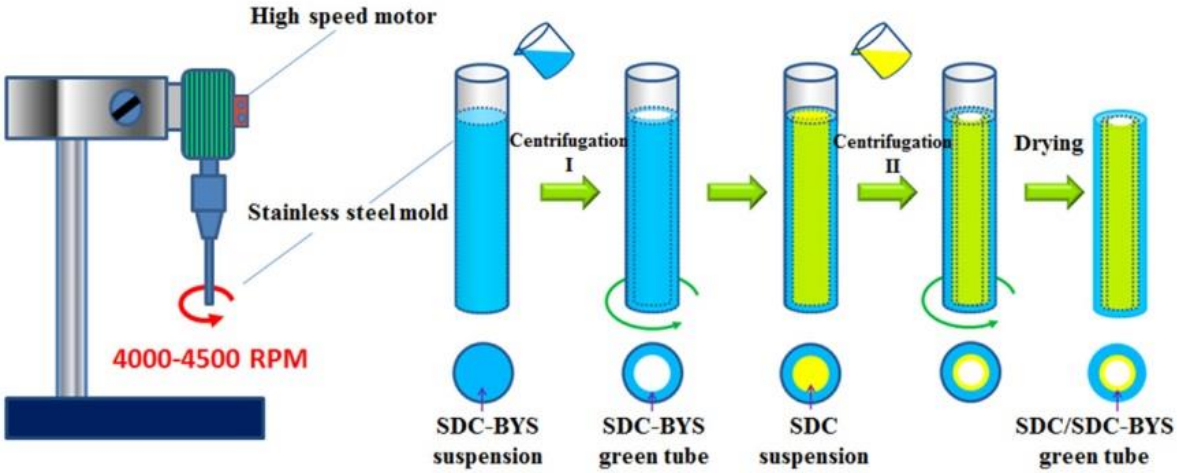

***Figure 21**: Schematic of the preparation process of tubular asymmetric SDC-carbonate dual phase membrane by centrifugal casting method.*

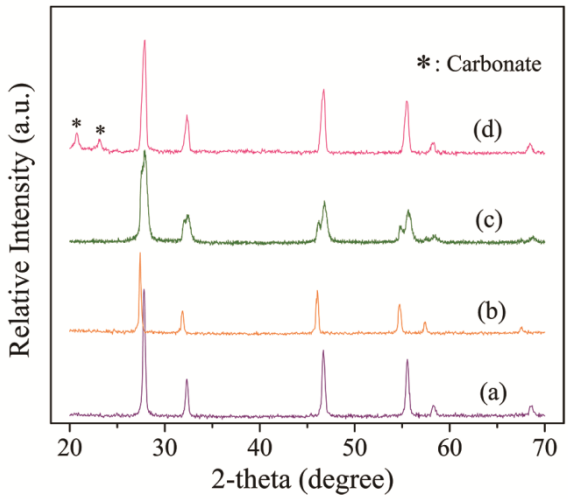

***Figure 22:** XRD patterns of (a) SDC powders calcined at 900 ^{o}C; (b) BYS powders calcined at 900 ^{o}C; (c) SDC-BYS porous support sintered at 1120 ^{o}C; (d) SDC-carbonate dual phase membrane.*

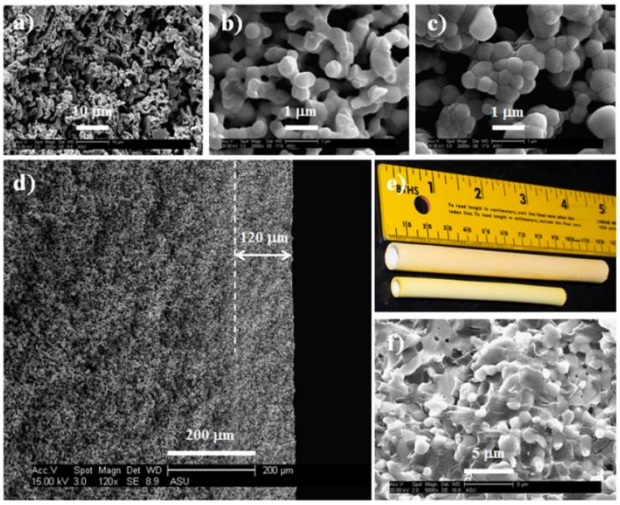

***Figure 23:** SEM images of asymmetric SDC/BYS-SDC substrate and membrane: (a) cross section of BYS-SDC layer; (b) cross section of SDC layer; (c) inner surface of SDC layer; (d) cross section of the asymmetric SDC/BYS-SDC substrate; (e) photo of SDC/BYS-SDC substrates with different sizes; (f) cross section of the SDC layer after infiltration.*

6. Results of Task D: Gas Separation and Stability Study on Tubular and Disk Membranes

6.1 Gas Separation of Tubular Dual Phase Membranes

CO_2 separation performance of tubular ceramic-carbonate dual phase membranes was analyzed on a high temperature gas permeation setup as shown in **Figure 24**. CO_2 and N_2 were introduced into the tube side of the membrane. CO_2 transported through the membrane to the permeate side and was swept out by helium. Both feed side and permeate side gases were fed tp the GC for composition analysis. Two different modules can be used in this setup: 1) stainless steel module with graphite gaskets for sealing, test temperature up to 700 ^oC, high feed pressure can be introduced; 2) ceramic module with ceramic-glass mixture for sealing, test temperature up to 950 ^oC, feed and sweep sides keep at atmospheric pressure. The ceramic module can also be used for membrane reactions. For example, the CO_2 can be changed to be syngas in the feed and water was introduced into the feed side by a syringe pump. The WGS reaction occurred at the tube side. The produced CO_2 permeated through the membrane to the outer side and was swept out the by the helium. After removing the steam by the cold trap, the gases were introduced into the GC for composition analysis.

The CO_2 separation performance of tubular symmetric (with the thickness of 1.5 mm) and asymmetric (with the thickness of SDC layer of 150 μm and the porous support layer of about 1.4 mm) SDC-carbonate dual phase membranes were tested [45]. As shown in **Figure 25**, Both CO_2 flux and permeance increase with increasing temperature. At 900 ^oC, the CO_2 flux and permeance of the asymmetric membrane are 1.56 ml cm^{-2} min^{-1} and 2.33×10^{-7} mol m^{-2} s^{-1} Pa^{-1}, respectively, which are 3 times that of the symmetric membrane. At 800 ^oC, the difference reaches 3.6 times. The results further confirm that reducing the thickness of the membrane is an effective route to improve the CO_2 permeation performance. Because of the gas transport resistance of the porous SDC-BYS support, the increase of CO_2 flux and permeance is not as large as the reducing of membrane thickness (nearly 10 times). For the symmetric membrane, the CO_2/N_2 selectivity is higher than 200. For the asymmetric membrane, the selectivity is higher than 50.

The CO_2 permeation activation energy of the asymmetric membrane is about 60.3 kJ mol^{-1} (**Figure 26**), which is lower than that of the symmetric tubular membrane (81.2 kJ mol^{-1}) but close to that of the reported disk thick membrane with similar SDC and carbonate composition [46]. The difference of the activation energy may be caused by the different microstructure of the SDC substrate. The asymmetric SDC/SDC-BYS substrate sintered at lower temperature (1120 ^oC) than the symmetric SDC substrate (1420 ^oC), therefore the porosity is relatively high, leading to high ratio of carbonate to SDC in the membrane. The high relative amount of carbonate in the membrane results in low CO_2 permeation activation energy because the activation energy of carbonate ionic conducting via carbonate phase is lower than that of oxygen ionic conducting via SDC phase [47].

Beside the CO_2/N_2 separation, the symmetric SDC-carbonate membrane was also used for the separation of CO_2 from simulated syngas with the composition of 49.5% CO, 36% CO_2, 10% H_2 and 4.5% N_2. The CO_2 separation performance of the symmetric tubular membrane is

show in **Figure 27**. Both CO_2 permeation flux and permeance increase with increasing the temperature. At 900 ^oC, the CO_2 permeation flux and permeance are 0.38 ml cm^{-2} min^{-1} and 1.05×10^{-7} mol m^{-2} s^{-1} Pa^{-1}, respective. At 800 ^oC, that is 0.18 ml cm^{-2} min^{-1} and 4.39×10^{-8} mol m^{-2} s^{-1} Pa^{-1}, respective. In the feed side, the concentration of CO_2 is about 35%. In our previous work, we also tested the CO_2 separation performance of the tubular SDC-carbonate membrane with a CO_2 feed concentration of 40% at 900 ^oC. We found that the CO_2 permeation flux and permeance are 0.44 ml cm^{-2} min^{-1} and 0.86×10^{-7} mol m^{-2} s^{-1} Pa^{-1}, respective. Generally, the CO_2 permeation flux increases while the permeance decreases with increasing the CO_2 feed concentration. Therefore, no obvious difference in the membrane separation performance is observed under syngas atmosphere. CO_2/N_2 and CO_2/H_2 selectivities are about 200 and 65, respectively. The CO_2 permeation activation energy of the symmetric tubular membranes is 89.62 kJ mol^{-1} (**Figure 28**), similar to that in the CO_2/N_2 atmosphere (**Figure 26**).

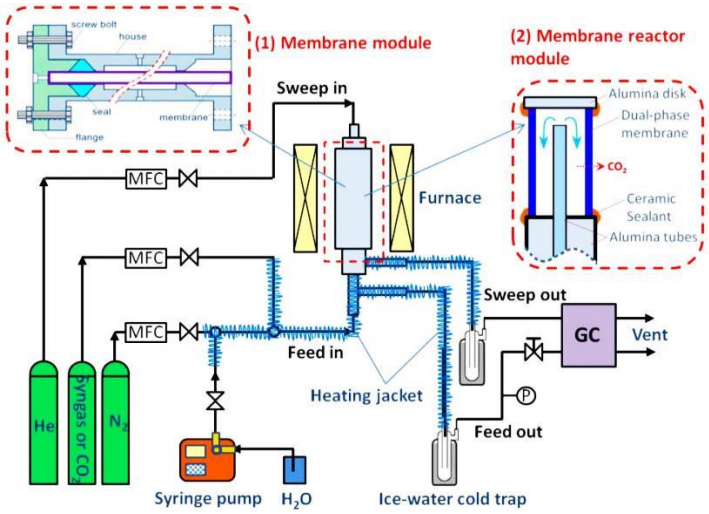

Figure 24: *Schematic of high temperature CO_2 permeation setup for tubular membranes.*

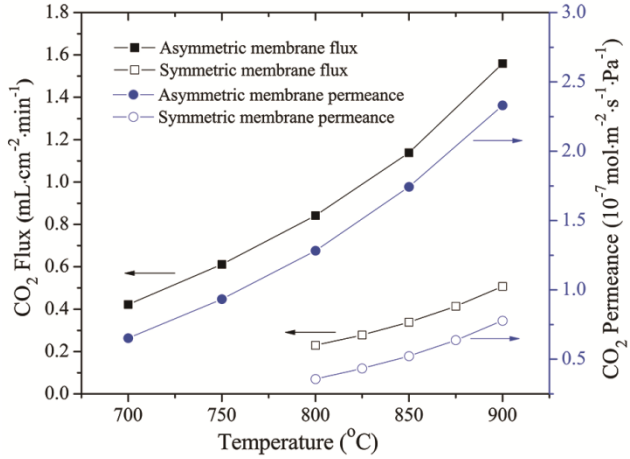

Figure 25: *CO_2 permeation flux and permeance of asymmetric and symmetric tubular dual-phase membranes as a function of temperature. Feed side: CO_2 flow rate 25 ml min^{-1}, N_2 flow rate 25 ml min^{-1}; Sweep side: He flow rate 50 ml min^{-1}.*

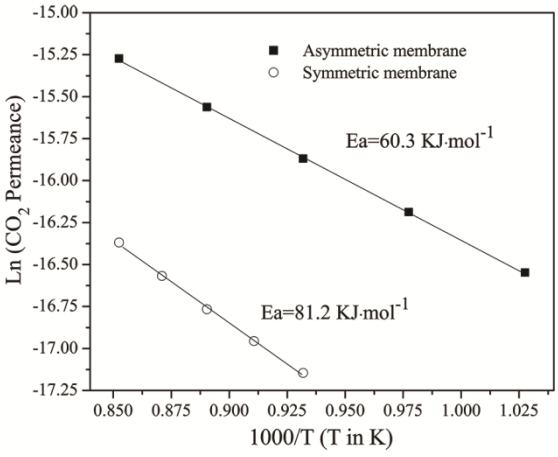

Figure 26: *Arrhenius plot of the thin and bulk tubular dual-phase membranes. Feed side: CO_2 flow rate 25 ml min^{-1}, N_2 flow rate 25 ml min^{-1}; Sweep side: He flow rate 50 ml min^{-1}.*

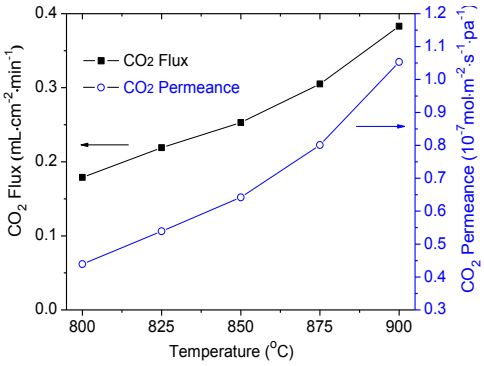

Figure 27: *CO_2 permeation flux and permeance of symmetric SDC tubular dual-phase membrane as a function of temperature. Feed side: syngas flow rate 100 ml min^{-1}; Sweep side: He flow rate 100 ml min^{-1}. Thickness of the membrane is about 1.5 cm. Total pressure at feed and permeate sides are both 1 atm.*

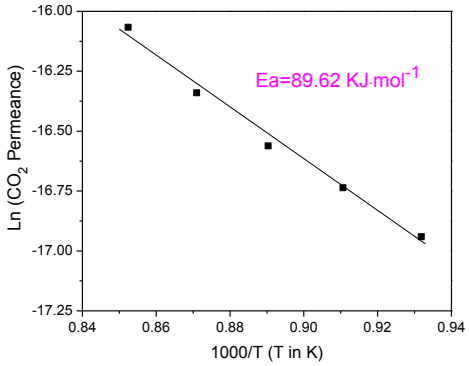

Figure 28: *Arrhenius plot of the symmetric SDC tubular dual-phase membranes. Feed side: syngas flow rate 100 ml min^{-1}; Sweep side: He flow rate 100 ml min^{-1}. Thickness of the membrane is about 1.5 cm. Total pressure at feed and permeate sides are both 1 atm.*

6.2 Long-Term Stability of Disk Dual Phase Membranes

For practical application of the dual phase membrane in pre-combustion CO_2 capture, good stability of the membrane for long-term operation is very important. At first, the stability of the disk SDC-carbonate membrane for CO_2/N_2 separation was tested. As shown in **Figure 29**, the SDC-carbonate membrane was operated for 14 days, and then at day 15, CO_2 was turned off in the feed for exactly two hours. The CO_2 permeation flux sees a drop of about 20%, before recovering back to approximately 90% of the initial value. These results showed on one hand that the SDC-carbonate membrane is very stable by maintaining a high permeation flux with no sign of decomposition for one month; and on the other hand that it has the capability to recover itself to a certain extent when exposed to a low CO_2 partial pressure below the equilibrium partial pressure of carbonate decomposition. In contrast, the disk LSCF membrane can only be tested for 4 days.

In addition, the long-term CO_2 permeation property of the disk SDC-carbonate membrane with a simulated syngas feed (49.5% CO, 36% CO_2, 10% H_2 and 4.5% N_2) was also investigated [40]. 1.5 mm thick disk SDC-carbonate membrane was used for the tests at 700 ^oC, and the results are given in **Figure 30**. As shown, this membrane was operated under the syngas environment for 35 days and the CO_2 permeation flux maintained stable. At approximately day 10 we observed a decrease in permeation flux which continued until approximately day 17 resulting in a decrease in flux of 20%. From this point, we found a slight recovery for the duration of the next testing, reaching 90% of the original flux. The reason for this trend is unclear at this time. Possible explanations include a combination of changes in surface structure, carbonate thickness, and the permeation experimental setup itself. This result indicates that the SDC-carbonate dual-phase membranes are very stable even under syngas environment. The

reducing conditions did not show obvious impact on the stability of the membrane. Membranes exposed to a total feed pressure of 5 atm reach a higher permeation flux of over 0.4 mL·cm^{-2}·min^{-1} after 5 days of test.

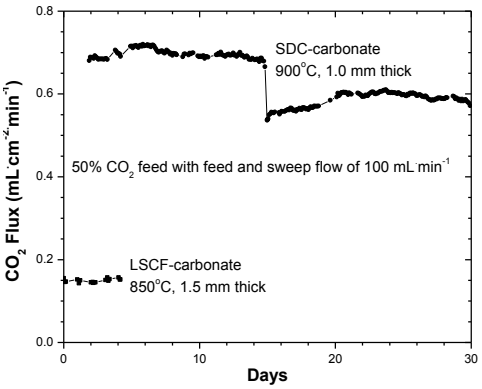

***Figure 29**: Stability of disk SDC-carbonate and LSCF-carbonate dual-phase membranes for CO_2/N_2 separation at 900 ^oC.*

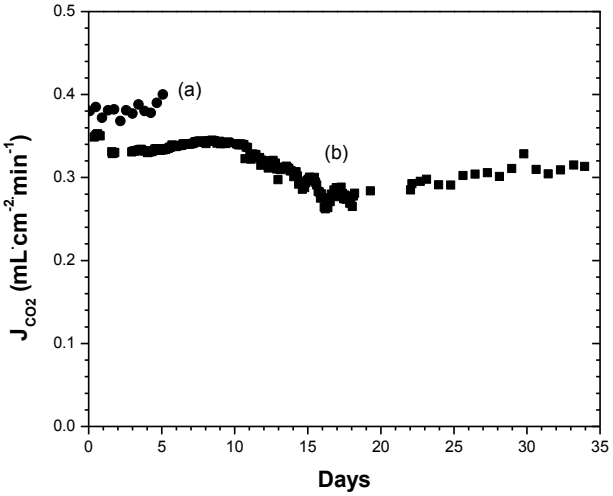

***Figure 30**: Time dependence of CO_2 permeation flux of SDC-carbonate membranes with simulated syngas feed at 700 ^oC: (a) high pressure feed at total feed pressure of 5 atm and CO_2 partial pressure of 1.8 atm; (b) atmospheric pressure feed with CO_2 partial pressure of 0.35 atm.*

7. Results of Task E: Synthesis and WGS Reaction Kinetic Study of High Temperature Catalyst

A modified Fe-based spinel-type oxide catalysts (Fe-Cr-Cu with the atomic ratio of 10:1:0.25) for high temperature WGS reaction was synthesized by ammonia assisted co-precipitation method [48]. Typically, a predetermined amount of metal nitrates was dissolved in de-ionized water. After that, a dilute aqueous ammonia solution was gradually added drop-wise to the aforementioned mixture solution under vigorous stirring until co-precipitation is completed at a given pH. The precipitated gel was further aged overnight and filtered off, and the obtained solid resultant was dried at in air 80^{o}C. The catalyst was finally obtained by subsequent calcinations of the dried precursor at a high temperature for several hours in an inert environment.

For the kinetic study, a fixed-bed reactor was packed with the catalyst; the reactor was heated up to 200 ^{o}C under helium inert gas at a flow rate of 20 ml·min^{-1} to clean the catalyst. After that, helium inert gas was then stopped and a process gas containing 33.3% CO: 25.0% CO_2: 25.0% H_2: 16.7% steam with a reduction factor of R=1.4 was fed into the reactor to activate the catalyst. Catalyst activation was conducted at 400 ^{o}C for 4 h in the presence of the process gas. After activation, a series of experiments were conducted at 500 ^{o}C to determine the kinetic parameters of WGS reaction over the prepared catalyst.

There are many kinetic equations reported in the literature for different WGS catalyst systems. The following equation is one of the most common equations that have been used to describe the kinetic reaction of WGS reaction using iron-based high temperature WGS catalyst:

$$R = K_C \exp(\frac{-88 \pm 2.18}{R'T}) P_{CO}^a P_{H2O}^b P_{CO2}^c P_{H2}^d (1 - \frac{1}{K_e} \frac{P_{H_2} \cdot P_{CO_2}}{P_{CO} \cdot P_{H_2O}}) \quad (12)$$

where R is the WGS reaction rate (mol g^{-1} s^{-1}), R' is the gas constant, T is the temperature (K), K_e is the equilibrium constant of WGS reaction, which can be expressed as:

$$K_e = \exp(\frac{E_a}{T} + C) \quad (13)$$

As can be seen from Eq. (12), there are four independent parameters (reaction order a, b, c and d, for reacting gas CO, H_2O, CO_2 and H_2, respectively) in the kinetic equation. **Tables 4-7** show the experiments that has been designed and conducted to determine these kinetic parameters of WGS reaction over iron-based catalyst (total flow rate 80 cc/min). As can be seen from these tables, for each set of experiments, only the partial pressure of one reacting gas is changed while the others are kept constant. In this way, only one reaction order can be determined in each set of experiments by fitting the measured CO conversion rate into the following equation:

$$\ln(R/(1-\beta)) = \ln(K_C) + a\ln(P_{CO}) + b\ln(P_{H2O}) + c\ln(P_{CO2}) + d\ln(P_{H2}) \quad (14)$$

Tables 4-7 also show the four sets of CO reaction rates measured at different experimental conditions. Fitting each set of measured CO conversion rates into Eq. (14) gives the reaction order for each kind of reacting gas. **Figure 31** shows the ln-ln plots for the effect of gas partial pressure on the gas reaction rates of WGS reactions over iron-catalyst. The slopes of the curves give the reaction order of different gases. The obtained reaction orders for CO, H_2O CO_2 and H_2, during WGS reaction for hydrogen production are 0.890, 0.330, -0.0163 and -0.053, respectively.

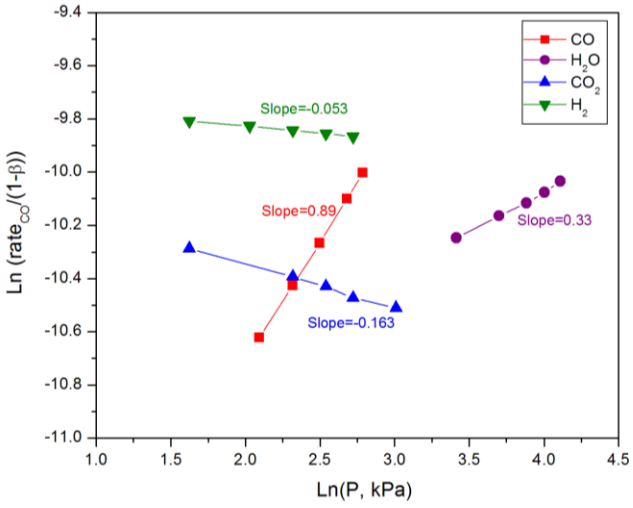

***Figure 31**: ln-ln plot for the effect of gas partial pressure on the gas reaction rates during WGS reaction over Fe-based catalyst.*

***Table 4**: Experiments to determine the reaction of CO.*

	P_CO (kPa)	**P_H_2O (kPa)**	**P_CO_2 (kPa)**	**P_H_2 (kPa)**	**P_N_2 (kPa)**	**CO conversion rate mol g^{-1} s^{-1}**
Exp. 1.1	16.212	60.795	10.132	10.132	4.053	0.00004413
Exp. 1.2	14.591	60.795	10.132	10.132	5.674	0.00003990
Exp. 1.3	12.159	60.795	10.132	10.132	8.106	0.00003362
Exp. 1.4	10.132	60.795	10.132	10.132	10.132	0.00002846
Exp. 1.5	8.106	60.795	10.132	10.132	12.159	0.00002317

***Table 5**: Experiments to determine the reaction order of H_2O.*

	P_CO (kPa)	**P_H_2O (kPa)**	**P_CO_2 (kPa)**	**P_H_2 (kPa)**	**P_N_2 (kPa)**	**CO conversion rate mol g^{-1} s^{-1}**
Exp.2.1	20.264	60.792	10.132	5.066	5.066	0.00004340
Exp.2.2	20.264	54.713	10.132	5.066	11.145	0.00004157
Exp.2.3	20.264	48.634	10.132	5.066	17.229	0.00003988
Exp.2.4	20.264	40.528	10.132	5.066	25.335	0.00003790
Exp.2.5	20.264	30.396	10.132	5.066	35.464	0.00003474

***Table 6**: Experiments to determine the reaction order of CO_2.*

	P_CO (kPa)	**P_H_2O (kPa)**	**P_CO_2 (kPa)**	**P_H_2 (kPa)**	**P_N_2 (kPa)**	**CO conversion rate mol g^{-1} s^{-1}**
Exp. 3.1	10.132	60.792	5.066	5.066	20.264	0.00003373
Exp. 3.2	10.132	60.792	10.132	5.066	15.198	0.00003006
Exp.3.3	10.132	60.792	12.665	5.066	12.665	0.00002882
Exp. 3.4	10.132	60.792	15.198	5.066	10.132	0.00002747
Exp. 3.5	10.132	60.792	20.264	5.066	5.066	0.00002619

***Table 7**: Experiments to determine the reaction order to H_2.*

	P_CO (kPa)	P_H_2O (kPa)	P_CO_2 (kPa)	P_H_2 (kPa)	P_N_2 (kPa)	CO conversion rate mol g^{-1} s^{-1}
Exp. 4.1	15.198	60.792	5.066	5.066	15.198	0.00005461
Exp. 4.2	15.198	60.792	5.066	7.599	12.665	0.00005342
Exp. 4.3	15.198	60.792	5.066	10.132	10.132	0.00005238
Exp. 4.4	15.198	60.792	5.066	12.665	7.599	0.00005156
Exp. 4.5	15.198	60.792	5.066	15.198	5.066	0.00005082

8. Results of Task F: Modeling and Analysis of Dual-Phase Membrane Reactor for WGS

8.1 Modeling WGS Reaction in Dual-Phase Membrane Reactor with CO_2 Recovery

A mathematical model for WGS reaction in the dual-phase membrane reactor was set up. The membrane reactor is in a tube-and-shell reactor configuration, where a WGS catalyst is packed in the tube side. Reforming gas is fed to the tube side, and the nitrogen is set to the shell side of the membrane reactor. Mass balance gives the following differential equations. For the tube side:

$$\frac{dq_i}{dz} = \pi R^2 \rho_B \nu_i \gamma - 2\pi R F_i \Delta P_i \qquad (15)$$

where q_i (i= CO, H_2O, CO_2, H_2, N_2) is the molar flow rate in the tube side, v_i the stoichiometry of species i in WGS reaction, v_{N2} = 0, F_i is permeance for species i, ΔP_i is the partial pressure difference of species i between the tube side and the shell side, and γ is the reaction rate for WGS.

For the shell side:

$$\frac{dQ_i}{dz} = 2\pi R F_i \Delta P_i \qquad (16)$$

where Q_i is the molar flow rate in the shell side.

The kinetic equation Eq. (12) for WGS reaction on the Fe-based spinel-type oxide catalysts in the tube side was used. Values for the parameters in Eq. (12) were obtained by fitting experimental data, as discussed in section 7.

At first, a theoretical model Eq. (7) for CO_2 permeation flux through the ceramic-carbonate dual-phase membrane consisting of mixed-conducting oxide ceramic and molten carbonate phases was used. The theoretical CO_2 permeation equation obtained for the case of pure CO_2 permeation is shown below:

$$J_{CO2} = [\frac{\varepsilon}{\tau}]_{MC} \frac{RT\phi\sigma_i}{4F^2L} \ln\left(\frac{P_{CO2(tube)}}{P_{CO2(shell)}}\right) \quad (17)$$

Permeation flux is zero for other species. In Eq. (17), $[\varepsilon/\tau]_{MC}$ is the porosity and tortuosity factor for the SDC support. Since the support pores are filled with carbonate, these two properties represent transport of carbonate in the carbonate phase. The ratio $[\varepsilon/\tau]_{MC}$ is measured by room temperature helium permeation testing. Furthermore, ϕ and σ_i are the geometric correction factor and oxygen ionic conductivity for the solid phase of the porous SDC support. CO_2 permeation flux equation Eq. (17) was used in this modeling. The ionic conductivity values of SDC as a function of the temperature were adopted from the literature [49], and were directly used in the model for simplicity. Other variables related with the membrane features such as membrane thickness (L) and volume fraction of each phase were taken from experimental results. In **Table 8** the main reference parameters used in this modeling are summarized.

***Table 8**: Membrane parameters used in this modeling*

Parameter	Reference value
(ε/τ)	0.11
ϕ	0.7
L (membrane thickness)	1.5 mm
Ionic conductivity of SDC (σ_i)	σ_i=224.6exp(-9051.5/T);T=400-700°C (S/cm) [49]
R	8.314 J/mol K
F (Faraday constant)	96485.336 C/mol

A series of ordinary differential equations with initial conditions at $z = 0$ were solved using a numerical Runge-Kutta method. The calculation was performed on the Matlab.

8.2 Modeling Results and Analysis

Modeling results in a dual-phase membrane reactor were calculated by considering that the length of the membrane is 1.0 cm, the weight of catalyst is 0.4 g, the flow rate of CO is 15 ml min^{-1}, H_2O/CO ratio is 3.0 and a sweep gas flow rate of 30 ml min^{-1}. We find that the CO conversion in membrane reactor is similar with that in fixed bed reactor even under high feed pressure (10 atm). This is caused by the relatively low CO_2 permeation flux (CO_2 permeance is lower than 5×10^{-8} mol $m^{-2}\cdot s^{-1}\cdot Pa^{-1}$ at 500 °C) of the dual-phase membrane at this operation condition.

To evaluate the modeling results under high CO_2 permeation flux, we assumed that the CO_2 flux is 10 times of the present values and the feed pressure is 5 atm (CO_2 permeance about 5×10^{-7} mol $m^{-2}\cdot s^{-1}\cdot Pa^{-1}$ at 500 °C). The modeling results are shown in **Figure 32**. Both CO conversion and CO_2 recovery increase with increasing the temperature (**Figure 32a**). At 520 °C, the CO_2 recovery reaches 80%. In addition, the CO conversion is higher than 95%, when the H_2O/CO ratio ≥3.0 and the temperature ≥500 °C (**Figure 32b**). In real case, however, the CO_2 permeance of the SDC-carbonate membrane cannot reach 5×10^{-7} mol $m^{-2}\cdot s^{-1}\cdot Pa^{-1}$ at 500 °C. Therefore, the WGS membrane reactor has to operate at higher temperatures (> 800 °C). At such high temperatures, the present WGS catalyst cannot be used. So, new WGS reaction kinetic equation should be developed.

Recently, the high temperature homogeneous WGS reaction in Pd-based membrane reactors without catalyst was proposed by the researchers at US National Energy Technology Laboratory (NETL) [50-52]. According to their results, a homogeneous WGS reaction kinetic equation was developed as Eq. (18) [52]

$$\gamma = Fk_f[CO]^{0.5}[H_2O](1 - \frac{[CO_2][H_2]}{K_{eq}[CO][H_2O]}) \qquad (18)$$

where F is a correction factor used to account for the catalytic activity of membrane materials, k_f is the forward reaction rate constant based on the study of Bustamante et al.[51], K_{eq} is the temperature-dependent WGS equilibrium constant, see Eq. (13). In addition, according to our new research results, a modified CO_2 permeation equation was developed as Eq. (10).

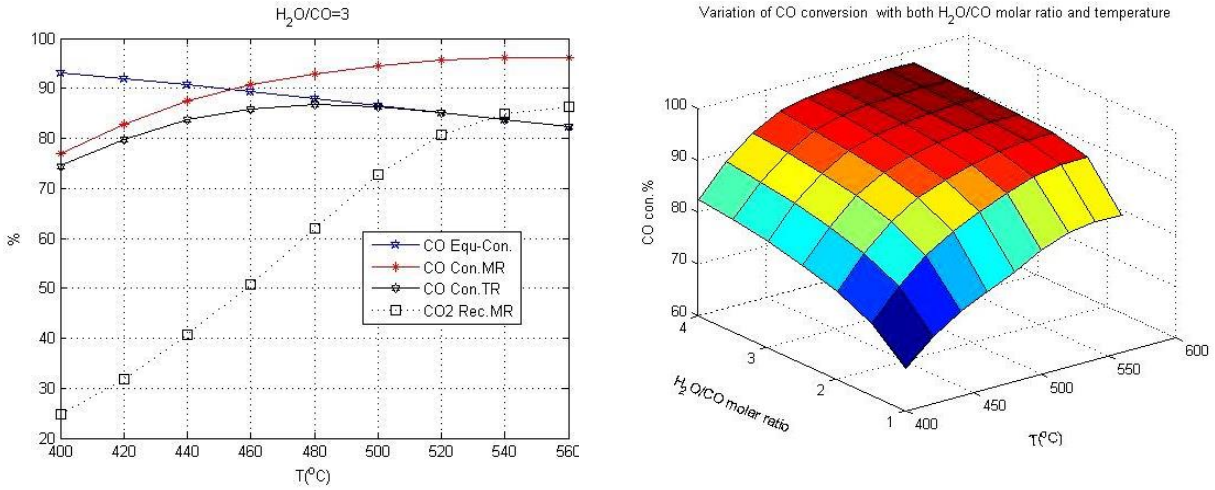

(a) (b)

***Figure 32**: (a) Equilibrium CO conversion, CO conversion in fixed bed reactor, CO conversion in membrane reactor and CO_2 recovery as a function of reaction temperature, H_2O/CO ratio is 3.0; b) CO conversion as a function of H_2O/CO ratio and temperature in the membrane reactor. Feed pressure is 5 atm. (the CO_2 permeation flux ×10)*

Based on the new kinetic equation and CO_2 permeation equation, the WGS reaction performance in the dual-phase membrane reactor without catalyst was recalculated, and the results are shown in **Figure 33**. The CO conversion in the dual-phase membrane reactor (MR) is higher than that in traditional reactor (TR), indicating that the membrane really shows contribution to the conversion of CO. However, both of them are much lower than the equilibrium conversion. Due to the limitation of reaction equilibrium especially at high temperature and without catalyst, the CO conversion is lower than the equilibrium conversion.

To verify the reliability of the modeling results, the experimental data of WGS reaction are also included in **Figure 33a**. The experimental data show the similar trends with that of the modeling results. The experimental CO conversion is a little bit higher than the modeling data especially at relatively low temperatures, which may be caused by the high activation energy in Eq. (18), 288.3 kJ/mol [51]. In contrast, the experimental CO_2 recovery is close to the modeling data. From **Figure 33b**, the CO conversion increases with increasing H_2O/CO ratio, which is consistent with the experimental results. Therefore, the improved model is reliable and can be used to predict the WGS membrane reactor performance under optimized conditions, such as high pressure.

8.3 Prediction of WGS Reaction Performance under Industrial Relevant Conditions

In the practical IGCC process, gasifier raw syngas containing CO, H_2, CO_2 etc, instead of pure CO is the feed for WGS reaction. Therefore, in this project, the model was used to optimize the WGS reaction with the raw syngas as the feed and identify experimental conditions for the membrane reactor to produce hydrogen stream in the retentate with high hydrogen purity (dry based).

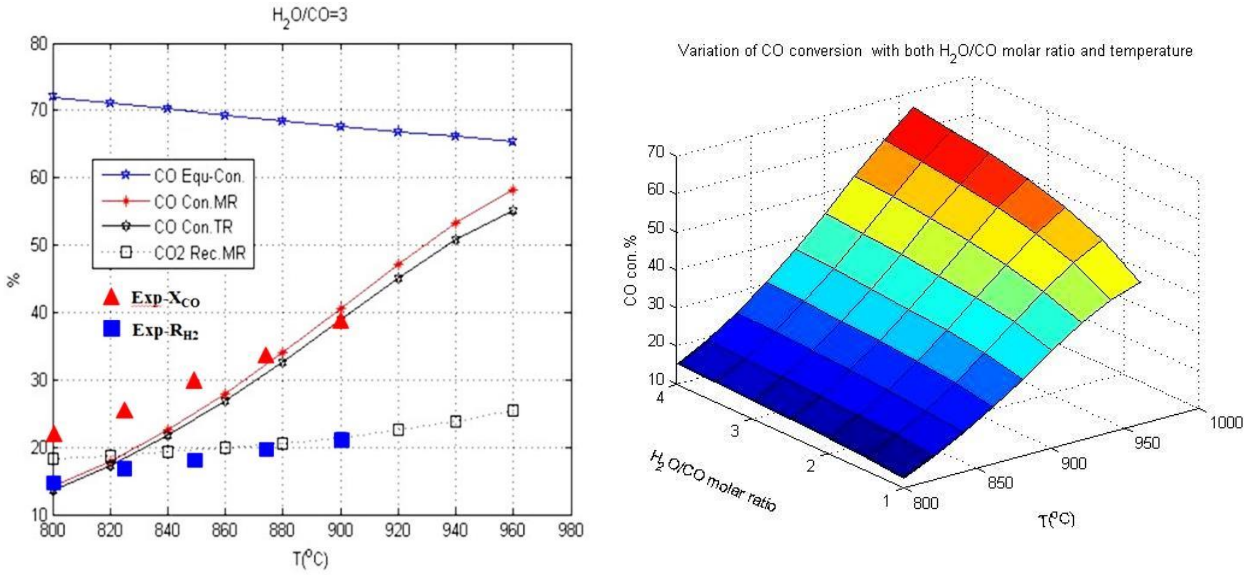

(a) (b)

***Figure 33**: (a) Calculated equilibrium CO conversion, CO conversion in traditional reactor (TR), CO conversion and CO_2 recovery in dual-phase membrane reactor (MR) and experimental results of CO conversion and CO_2 recovery in MR as a function of reaction temperature; (b) Calculated CO conversion as a function of H_2O/CO ratio and temperature in the MR. The feed pressure is 1 atm, H_2O/CO ratio is 3.0.*

The WGS reaction conditions for modeling calculation are listed in **Table 9**. In the dual-phase membrane reactor, high operation pressure at the reaction side (feed side) is beneficial for the transport of the produced CO_2 through the membrane, resulting in the shift of the reaction equilibrium toward CO_2 production, promoting the CO conversion. Therefore, feed pressure is an important factor for WGS reaction in membrane reactor with CO_2 removal. As shown in **Figure 34**, as the pressure increases from 1 to 40 atm, CO conversion increases from 26.5% to 48.7%, the CO_2 recovery increases significantly from 16.5% to 78.4%. These results show the great contribution of the dual-phase membrane to CO conversion. In addition, the high pressure promotes the CO_2 removal through the membrane, resulting in high H_2 concentration in the retentate (63.1% at 40 atm).

***Table 9**: WGS reaction conditions for modeling calculation.*

Temperature (^oC)	900
Feed pressure (atm)	1-40
Sweep side pressure (atm)	1
Catalyst	No
Syngas composition	56.5% CO, 8.2% CO_2, 35.3% H_2
Feed side syngas flow rate (mL min^{-1})	10-40
Syngas space velocity (min^{-1})	7.96-31.83
Steam to CO molar ratio	3.0
Sweep side He flow rate (mL min^{-1})	60

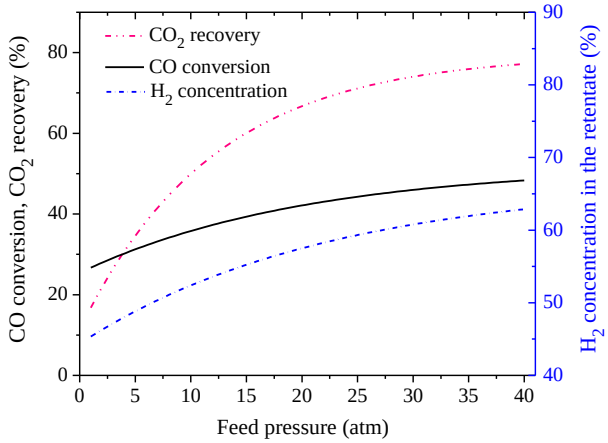

***Figure 34**: CO conversion, CO_2 recovery and H_2 concentration in the retentate as a function of feed pressure. Steam to CO ratio is 3.0; syngas flow rate 25 mL min^{-1}; syngas space velocity 19.89 min^{-1}; reaction temperature is 900 ^oC.*

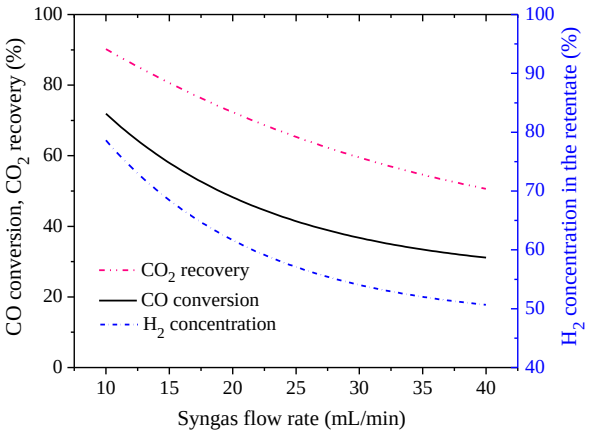

***Figure 35**: CO conversion, CO_2 recovery and H_2 concentration in the retentate as a function of syngas flow rate. Syngas space velocity 7.96-31.83 min^{-1}; Steam to CO ratio is 3.0; reaction temperature is 900 ^oC; feed pressure is 20 atm.*

The effect of syngas flow rate on WGS reaction performance was also studied, as shown in **Figure 35**. CO conversion, CO_2 recovery and H_2 concentration in the retentate decrease with increasing the syngas flow rate. When syngas flow rate is 10 mL min^{-1}, space velocity of 7.96 min^{-1}, the CO conversion, CO_2 recovery and H_2 concentration in the retentate are 72.0%, 90.2% and 78.7%, respectively. However, the higher syngas flow rate reduces the residence time for WGS reaction, resulting in the decrease of CO conversion. Additionally, the higher syngas flow rate has adverse effect on CO_2 removal through the membrane because the relatively low CO conversion means low CO_2 partial pressure in the feed side and low CO_2 flux. Therefore, the role of the dual-phase membrane in the membrane reactor is also restrained at high syngas flow rate. From these results, the match between the syngas flow rate and the WGS reaction rate, and the match between the CO_2 production rate and the CO_2 removal rate through the membrane are key to ensure optimum operation of the membrane reactor.

8.4 Multi-Stage Syngas WGS Membrane Reactor

One of the objectives of this project is to identify optimum conditions for WGS reaction in the dual-phase membrane reactor to obtain H_2 and CO_2 streams with 93% and 95% purity, respectively. Since the CO_2 theoretical selectivity of the dual-phase membrane is 100%, 95% CO_2 stream at the permeate side can be obtained if the membrane without defects and the sealing of the reactor is good enough. In our work, the measured concentration of CO_2 is higher than 99% (without sweep gas). From section 8.3, however, the H_2 concentration in the retentate of a single-stage membrane reactor cannot reach 93% even at high temperature, under relatively high pressure, with relatively high steam to CO ratio, and low syngas flow rate.

In order to address this problem, we design a new multiple-stage syngas WGS membrane reactor, as shown in **Figure 36**. The raw syngas is introduced into the first stage of the reactor. Steam is added at the feed side to keep a fixed steam to CO ratio. The retentate is fed to the next stage of the membrane reactor. Each stage is operated at same temperature.

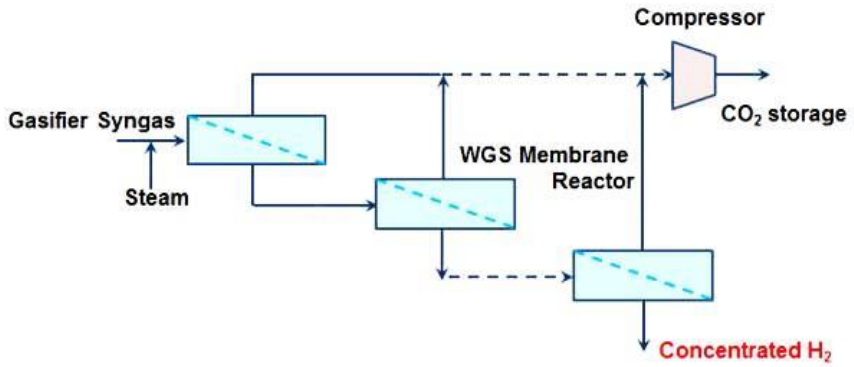

***Figure 36**: Schematic of multi-stage syngas WGS membrane reactor.*

Simulated raw syngas at the flow rate of 20 mL min^{-1} was introduced into the reactor of the first stage. Steam was added at the feed side of the first stage to keep a steam to CO ratio of 3.0. The retentate from the first stage is fed to the next stage of the membrane reactor. Each stage was operated at 900 ^oC. As shown in **Figure 37**, the concentration of H_2 at the reteante increases with increasing the reactor stages, while the CO and CO_2 concentration decrease. At the fourth stage, the H_2 concentration in the retentate reaches 95.5% (>93%). The high concentration of H_2 in the retentate restrains the further conversion of CO. Therefore, the CO concentration in the retentate of the fourth stage is still not close to zero (4.2%).

Figure 38 shows the effect of feed pressure on the H_2 concentration at the retentate of each stage. When the reactor was operated at 1 atm, H_2 concentration in the retentate of the fifth stage is 63.7% and still lower than the target value (93%). At 10 atm, the H_2 concentration in the retentate of the fifth stage reaches 93.2%, higher than 93%. In contrast, under 30 and 40 atm, the H_2 concentrations of the third stage reach 94.2% and 94.9%. In other words, a three-stage membrane reactor operated at the feed pressure of ≥30 atm can produce hydrogen stream with the hydrogen purity higher than 93%. Therefore, high operation pressure is beneficial for production concentrated hydrogen at the retentate. To produce hydrogen stream with high purity is feasible in the multi-stage syngas WGS membrane reactor, especially under high feed pressure.

The results shown in **Figure 38** indicate that the dual-phase ceramic-carbonate membrane can be used as membrane reactor without catalyst at temperatures around 900°C for WGS. The multiple-stage membrane reactor can produce high pressure H_2 stream and atmospheric CO_2 stream with sufficiently high purity (>93% and >95% respectively). Avoiding the use of a catalyst could greatly simplify the process and reduce the costs of the membrane reactor process. Such a simplified multiple-stage reactor has potential to replace the existing WGS reactors and amine separator, reducing the costs of converting coal or natural gas to H_2.

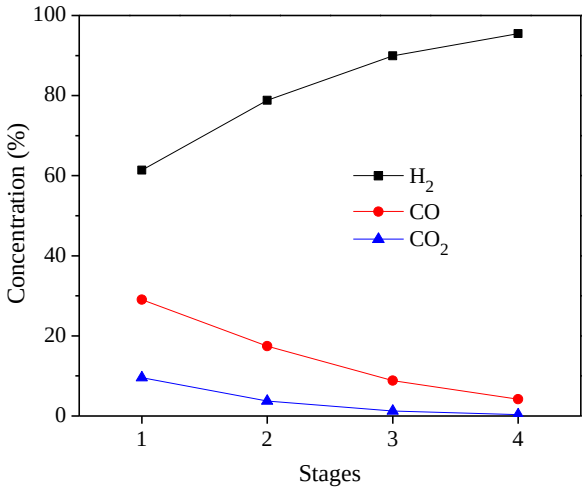

***Figure 37**: Concentration of various gases (without steam) in the retentate of different stages in the multi-stage WGS membrane reactor. The flow rate of syngas is 20 mL/min; Each stage is operated at 900 °C with the steam to CO ratio of 3.0 and under the feed pressure of 20 atm.*

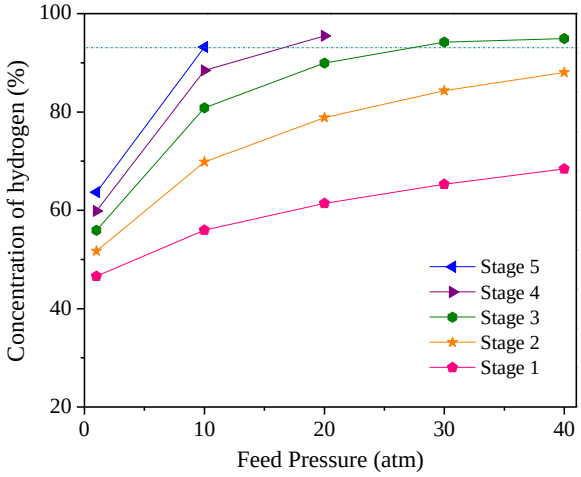

***Figure 38**: Concentration of hydrogen in the retentate of different stages in the multiple-stage WGS membrane reactor operated under various pressures. The flow rate of syngas is 20 mL/min. Each stage is operated at 900 °C with the steam to CO ratio of 3.0.*

9. Results of Task G: Experimental Studies on WGS in Dual-Phase Membrane Reactors

The high temperature WGS reaction experiments were conducted on a setup as shown in **Figure 24**. Nitrogen as a carry gas took steam and syngas (with the composition of 49.5% CO, 36% CO_2, 10% H_2 and 4.5% N_2) into the tube side of the tubular SDC-carbonate dual phase membrane, where the WGS reaction occurred. The produced CO_2 permeated through the membrane wall to the outer side and was swept out by helium.

First, the CO_2 permeation flux of the dual phase membrane during the syngas WGS reaction was measured (**Figure 39a**). CO_2 permeation flux increases upon increasing the temperature. At 900 °C, the flux is 2.7×10^{-3} mol m^{-2} s^{-1}. Compared with the CO_2 flux in CO_2/N_2 system (**Figure 25**), the relatively low flux in reaction process is attributed to the lower feed CO_2 concentrations [45]. During the reaction, the real feed CO_2 concentration was tested, which varies in the range of 12.6% to 14.8% depending on temperatures. In the membrane reactor, the activation energy for CO_2 permeation is estimated to be 90.8 kJ mol^{-1} (**Figure 39b**), which is a little bit higher than that in CO_2/N_2 system (83.3 kJ mol^{-1}, **Figure 26**). This is caused by the fact that the activation

energy for CO_2 permeation in the reaction process is also affected by the activation energy for CO_2 production from the WGS reaction, which is relatively high without catalyst [51].

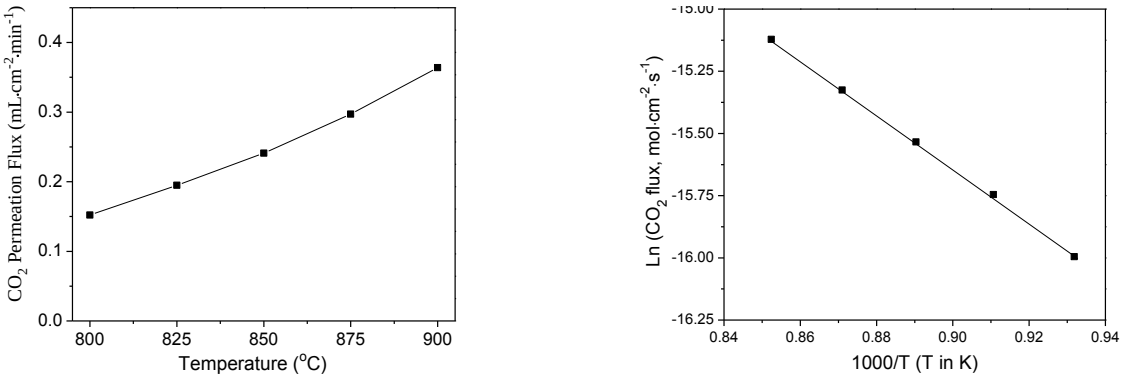

(a) (b)

Figure 39: *(a) CO_2 permeation flux of the SDC-carbonate tubular dual-phase membranes in syngas WGS reaction system; (b) Arrhenius plots of the CO_2 permeation flux for the dual-phase membrane. Feed side: syngas flow rate 20 mL min^{-1}, N_2 flow rate 10 mL min^{-1}, and H_2O (steam) to CO molar ratio is 3.0; Sweep side: He flow rate 60 mL min^{-1}. The pressure at feed and permeate sides are both 1 atm.*

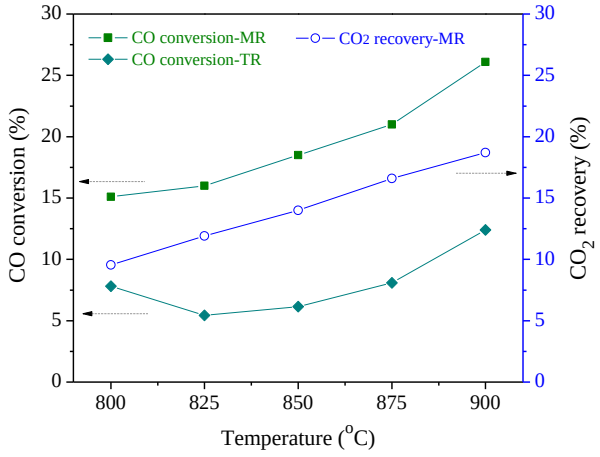

Figure 40: *Performance of dual phase membrane reactor (MR) and traditional reactor (TR) for syngas WGS reaction as a function of temperature without catalyst. Feed side: simulated syngas flow rate 20 mL min^{-1}, N_2 flow rate 10 mL min^{-1}, and H_2O (steam) to CO molar ratio is 3.0; Sweep side: He flow rate 60 mL min^{-1}. The pressure at feed and permeate sides are both 1 bar.*

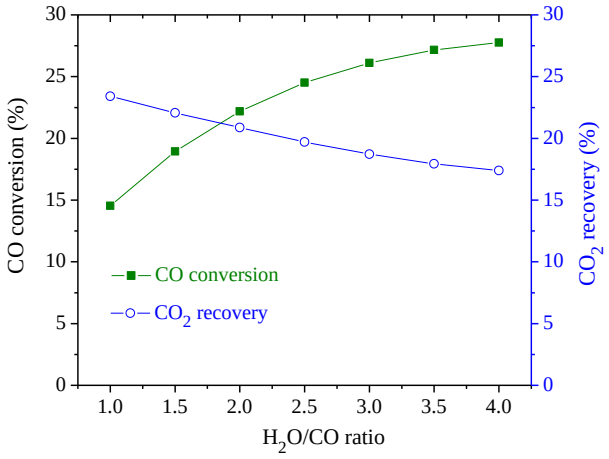

Figure 41*: Performance of dual phase membrane reactor as a function of steam to CO ratio at 900 °C. Feed side: simulated syngas flow rate 20 mL min^{-1}, N_2 flow rate 10 mL min^{-1}; Sweep side: He flow rate 60 mL min^{-1}. The pressure at feed and permeate sides are both 1 bar.*

For the high temperature syngas WGS reaction in the membrane reactor, temperature, steam to CO molar ratio and syngas flow rate are three critical parameters. Accordingly, the

effects of these parameters on the reaction performance were investigated. **Figure 40** shows the temperature dependence of reaction performance of the dual phase membrane reactor. CO conversion and CO_2 recovery increase from 15.1% to 26.1% and 9.6% to 18.7%, respectively, as the temperature increase from 800 to 900 ^oC. The WGS reaction is an exothermal reaction, thus the high temperature is adverse for the conversion of CO. However, the in situ removal of CO_2 by the dual-phase membrane greatly promotes the shifting of the reaction equilibrium. The increase of CO_2 permeation flux with temperature results in the relatively high CO conversion at high temperature. For comparison, the results of a traditional reactor (a dense alumina tube with the same size) measured at the identical conditions are also provided in **Figure 40**. CO conversion of the traditional reactor is much lower than that of the membrane reactor. These results indicate that using SDC-carbonate dual phase membrane reactor for high temperature syngas WGS reaction with simultaneous CO_2 removal is technically feasible, and high temperature is favorable for the reaction.

Figure 41 presents the effect of steam to CO molar ratio (H_2O/CO ratio) on the reaction performance at 900 ^oC. Upon increasing the H_2O/CO ratio, the CO conversion increases, while the CO_2 recovery shows an opposite trend. When the H_2O/CO ratio is 4.0, the CO conversion reaches 27.8% but the CO_2 recovery is 17.4 %. The enhancement of CO conversation is more significant at the H_2O/CO ratio of 1.0-3.0. However, further increase of H_2O/CO results in a relatively slow increase of CO conversation. This is attributed to that high H_2O/CO ratio reduces the residence time of the feed gases in the reactor since the CO flow rate is fixed. As is well known, short residence time is unfavorable for both CO conversion and CO_2 recovery. In addition, excessive steam for the relatively high H_2O/CO ratio reduces the partial pressure of CO_2 in the reaction side, resulting in the low CO_2 permeation flux and low CO_2 recovery. Therefore, in following experiments, the H_2O/CO ratio is fixed as 3.0.

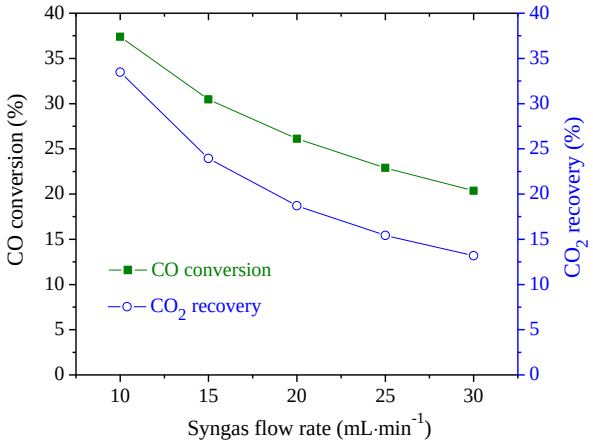

***Figure 42**: Performance of dual phase membrane reactor as a function of syngas flow rate at 900 ^oC. Feed side: simulated syngas flow rate 10-30 mL min^{-1}, N_2 flow rate 10 mL min^{-1}, steam to CO ratio is 3.0; Sweep side: He flow rate 60 mL min^{-1}. The pressure at feed and permeate sides are both 1 bar.*

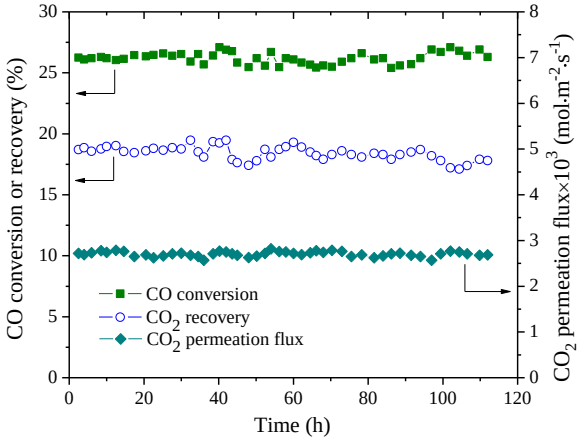

***Figure 43**: Long-term stability of SDC-carbonate tubular dual phase membrane reactor for syngas WGS reaction at 90 ^oC without catalyst. Thickness of the membrane is ~1.5 mm. Feed side: simulated syngas flow rate 20 mL min^{-1}, N_2 flow rate 10 mL min^{-1}, and H_2O (steam) to CO molar ratio is 3.0; Sweep side: He flow rate 60 mL min^{-1}. The pressure at feed and permeate sides are both 1 bar.*

Figure 42 shows the effect of syngas flow rate on the reaction performance at 900 ^{o}C. Both CO conversion and CO_2 recovery decrease upon increasing the syngas flow rate. When the flow rate is 10 ml ṁin^{-1}, the CO conversion and CO_2 recovery are 37.4% and 33.5%, respectively. However, the higher syngas flow rate increases the space velocity and reduces the residence time for WGS reaction, resulting in the decrease of CO conversion. Enick and coworkers [53] also observed that during the WGS reaction the CO conversion could be seriously reduced from 99.7% to 55% by decreasing the residence time from 2s to 0.7s. Additionally, the higher syngas flow rate has negative effect on CO_2 removal through the membrane. Too much unreacted CO and steam in the feed greatly reduces the CO_2 partial pressure, leading to the low CO_2 permeation flux and decrease in CO_2 recovery.

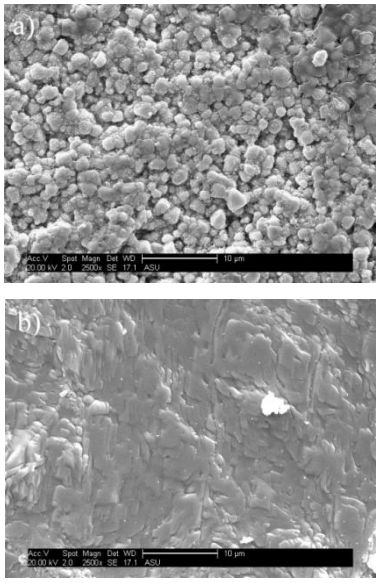

Figure 44: *SEM images of the SDC-carbonate membrane after long-term syngas water gas shift reaction: (a) outer surface (sweep side) and (b) inner surface (reaction side).*

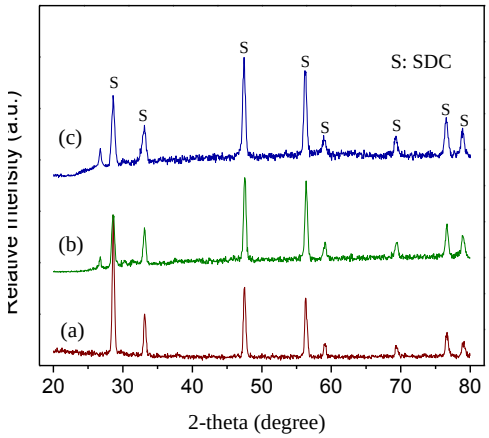

Figure 45: *XRD pattern of membrane after long-term syngas water gas shift reaction: (a) fresh membrane; (b) outer surface (sweep side); (c) inner surface (reaction side).*

For practical application of dual phase membranes, high thermal and chemical stability under harsh syngas WGS reaction environment is required. Furthermore, the thermal cycle stability is also an important factor should be considered in practical process. Therefore, the long-term stability of the SDC-carbonate membrane reactor was studied. First, the membrane was continuously operated for 30 h at 900 ^{o}C and then slowly cooling down to room temperature. After resealing, the membrane was heated to 900 ^{o}C for next test. Such a thermal cycle measurement was carried out for four times (0-30h; 30-58h; 58-84h; 84-112h). As shown in **Figure 43**, the CO conversion, CO_2 recovery and CO_2 flux maintain at around 26.2%, 18.4% and 2.7×10^{-3} mol ṁ$^{-2}$ s^{-1}, respectively. After long-term testing, the morphology of the membrane was analyzed (**Figure 44**). The surface of sweep side was slightly eroded, which may have been caused by the minor decomposition of carbonate under the low CO_2 partial pressure at high temperature. However, the thickness of the eroded layer is only 1-2 μm. In contrast, the surface of reaction side is dense and the corrosion of syngas and steam atmospheres to the membrane is

not obvious. The crystal structures of the membrane before and after long-term reaction were also analyzed (**Figure 45**). Both reaction side and sweep side maintain full fluorite structure. These results indicate that the SDC-carbonate dual phase membrane is stable under the syngas WGS reaction environment. Moreover, the membrane exhibits high thermal shock resistance. Accordingly, we can conclude that SDC-carbonate dual phase membrane has high potential for practical applications in high temperature CO_2 capture.

For possible industrial application of this new proposed process, the further improvement of CO conversion and CO_2 recovery is desired. Considering the membrane reactor feature, the one of the possible routes is increase the feed pressure. According to the modeling results in section 8.3, feed pressure is an important factor for WGS reaction in membrane reactor. To confirm the feasibility of this route, preliminary experiments of high pressure WGS reaction with CO and steam feed were conducted in a disk SDC-carbonate membrane reactor. The results are shown in **Table 10**. Both CO conversion and CO_2 recovery increase significantly upon increasing the feed pressure. At 700 ^oC, as the feed pressure increases from 1 to 5 bar, the increase of CO conversion and CO_2 recovery reach 51.2% and 453.5%, respectively. It is worth noting that the pressure of practical coal gasification gas may higher than 20 atm. Such a high feed pressure is of great benefit to the CO_2 removal through SDC-carbonate membrane, therefore facilitating the improvement of both CO conversion and CO_2 recovery.

***Table 10**: Performance of WGS reaction as a function of pressure at 700 ^oC without catalyst.**

Feed pressure (bar)	CO conversion (%)	CO_2 recovery (%)
1	44.4	2.8
2	55.7	8.1
3	61.2	11.5
4	65.0	13.8
5	67.3	15.5

** Thickness of the membrane is about 1.5 mm. Feed side: CO flow rate 10 ml/min, N_2 flow rate 40 ml/min, $H_2O/CO=3.0$; Sweep side: He flow rate 100 ml/min. The pressure at permeate sides is 1 bar.*

10. Results of Task H: Integration to IGCC and Economic Analysis

10.1 Design of Membrane Reactor for WGS and CO_2 Capture

A mathematical model for WGS reaction with CO_2 separation in the tubular membrane reactor was described in section 8 of this report. The model is a set of differential equations obtained from mass balance on gases in the reaction and sweep sides of the membrane, and includes equations for the homogeneous (catalyst-free) WGS reaction kinetics, and CO_2 permeation equation for the ceramic-carbonate dual-phase membrane obtained in this project. The solutions of the model, by Matlab, provide mass flow rates for H_2, CO, CO_2 and H_2O as a function of position of the tubular membrane reactor, including the values at the exit of the

reaction sweep sides of the membrane reactor. From the results obtained we can calculate the following parameters to indicate the reaction/separation target:

$$\text{Hydrogen Concentration, } (y_{H2(exit)}) = \frac{\text{Flow rate of } H_2 \text{ in retentate, } Q_{H2}(exit)}{\text{Total dry-based flow rate of the retentate, } Q_{total(d)}\ (exit)}$$

$$\text{Carbon Capture, CC\% } = \frac{\text{Flow rate of } CO_2 \text{ in the permeate, } Q'_{CO2}(exit)}{\text{Total carbon species flow rate in the feed, } Q_{CO}(feed)+Q_{CO2}(feed)}$$

At a given feed flow rate of coal syngas (and feed side pressure), the solution of the membrane reactor model provided dry-based hydrogen concentration and carbon capture percentage in the reactor effluents. Under specific conditions, one membrane tube (one stage) may not produce the product stream with hydrogen concentration or carbon capture that meet the desired target. In this case, multiple membrane tubes are connected in series (with respect to H_2 containing stream) to result in a multiple-stage membrane reactor for WGS with CO_2 capture. After extensive computational efforts, we found two-stage membrane reactor, as shown in **Figure 45**, would accomplish our separation targets.

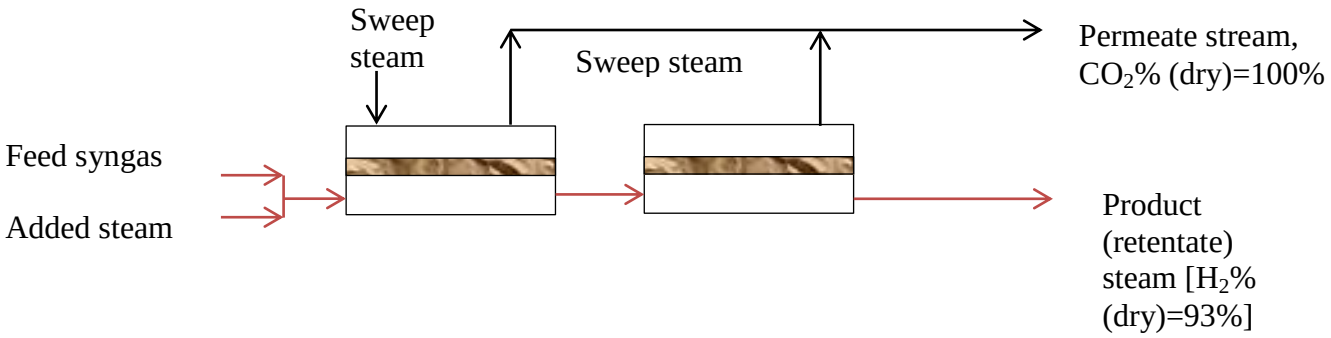

Figure 45 *Two-stage membrane tubes for high temperature water gas shift reaction with CO_2 separation*

If we chose 93% hydrogen concentration (dry-based) in the product (retentate) stream as the separation target, at 30 atm feed pressure the optimum condition stage number and coal syngas feed flow rate are 2 and 205 mL/min respectively. The performance results of the membrane reactor under such conditions are summarized in **Table 11**. As shown, the two-stage membrane reactor under such conditions can achieve 90.0% CO conversion and 90.2% CO_2 (carbon) captured, with product (hydrogen) stream containing 93% H_2 (dry-based), and permeate (carbon dioxide) stream containing 100% CO_2 (dry-based).

Table 11 also gives the mass balance results and compositions for the various streams shown in **Figure 45** which will treat coal syngas of the specific composition at flow rate of 205 mL/min. If the coal syngas at flow rate of 2050 mL/min should be treated, 10 two-stage membrane tubes in parallel should be used. Thus, the scaling up of the membrane reactor is accomplished by adding more membrane tubes connected in parallel.

It should be noted that a large amount of the steam is used for the sweep (low pressure steam, 1 atm), and for the feed (high pressure steam) to enhance WGS reaction rate and the driving force for CO_2 separation. Since WGS is exothermic reaction, heat should be removed from the reactor. Heat exchange in the membrane reactor can be challenging. It is suggested that we take advantages of these steam streams to remove the heat of reaction from the reactor.

Table 11 *Calculated Membrane Area and Reaction/Separation Performance of Ceramic-Carbonate Membrane Reactor for WGS and CO_2 Capture (based on a single two-stage tube)*

Parameter		Value
Membrane		
Inner diameter of membrane (cm)		0.8
Membrane length (cm)		100
Number of stages		2
Membrane area (based on average radius/inner radius) (cm^2)		592/502
Operation Conditions		
Operation Temperature (^oC)		850
Feed syngas flow rate (mL min^{-1})		205
Feed syngas composition (mol%) (other impurities: 1.1% H_2S, 0.8%N_2, 0.3% CH_4)	H_2	29.8
	CO	41.0
	H_2O	16.8
	CO_2	10.2
Flow rate of total added steam to the feed (mL. min^{-1})		218
Feed pressure (atm)		30
Sweep steam flow rate (each stage) (mL min^{-1})		200
Sweep side pressure (atm)		1
Reaction and Separation Performance		
CO conversion %		90.0
Permeate total flow rate (mL min^{-1})		495
CO_2 concentration in the permeate (dry-based) (mol%)		100
Permeate composition (wet-based) (mol%)	CO_2	19.1
	H_2O	80.9
Carbon capture %		90.2
Retentate (product) total flow rate (mL min^{-1})		323
H_2 concentration in retentate (product) (dry-based) (mol %)		93
Retentate composition (wet-based) (mol%)	H_2	42.23
	CO	2.6
	H_2O	54.6
	CO_2	0.5

10.2 Integration of Ceramic-Carbonate WGS Membrane Reactor with IGCC for CO_2 Capture

The process of the traditional WGS reaction for hydrogen production with CO_2 capture for IGCC power plant is described in **Figure 46**. The overall reaction/separation process for the IGCC power plant includes gasification, flyash removal, 2 or 3-fixed-bed reactors for water-gas-shift reaction (with at least two different catalysts), and H_2S and CO_2 removal by the low temperature process such as methanol washing (REACTISOL process). The catalyst for WGS should be sulfur resistant. **Figure 46** also shows temperatures of various units in the process and

heat exchanges required. The design of the process incorporating the ceramic-carbonate WGS membrane reactor into IGCC process is a modification of the conventional IGCC process shown in **Figure 46**. In order to provide comparison basis for the IGCC process with integration of the dual-phase ceramic membranes, we worked on the detailed design of the WGS reaction with CO_2 capture by Aspen HYSYS. The Aspen HYSYS process flow diagram (PFD) for the traditional WGS with CO_2 capture by our design is shown in **Figure 47**, which depicts all reaction, heat transfer, separation and auxiliary equipment utilized in the process.

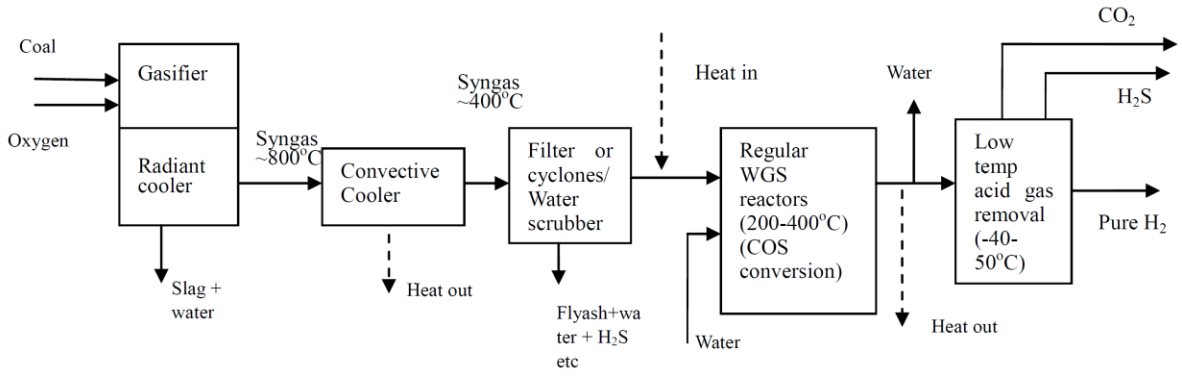

Figure 46. *Block-flow diagram of traditional WGS reaction with CO_2 capture for IGCC power plant*

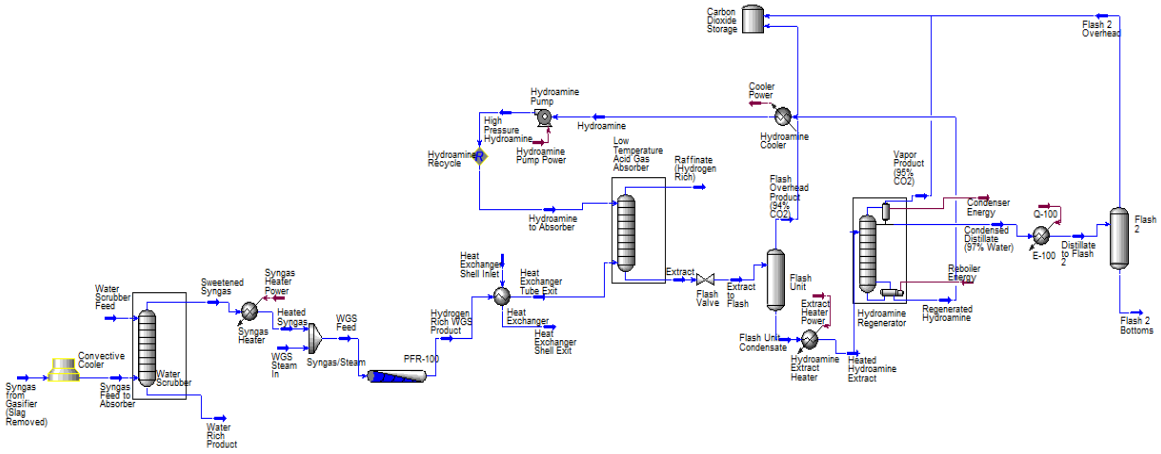

Figure 47 *Aspen HYSYS Process-flow-diagram of traditional WGS reaction with CO_2 capture for IGCC power plant*

Figures 48 and 49 show the reheated membrane WGS reaction process with CO_2 capture. The process has the ceramic-carbonate membrane reactor replacing the conventional fixed-bed WGS reactors and low-temperature CO_2 removal unit. It represents a significant simplification in the IGCC process. The new ceramic-carbonate membrane reactor is operated at temperatures as high as 800°C. Its advantages are elimination of WGS catalyst and simultaneous CO_2 separation with WGS reaction. CO_2 removal significantly reduces the amount of absorbent needed in the low temperature acid gas removal. The other advantage of this arrangement for the integration of the membrane reactor with the IGCC process for CO_2 capture is that most unit

operations in the IGCC process remain unchanged. The disadvantage is that the high operation temperature increases equipment and operating costs for heating and cooling the streams entering and leaving the membrane reactor. Heat contained within the WGS exit stream can be exchanged with utility water to generate steam needed for the permeate sweep. Heat integration is illustrated in **Figure 49**.

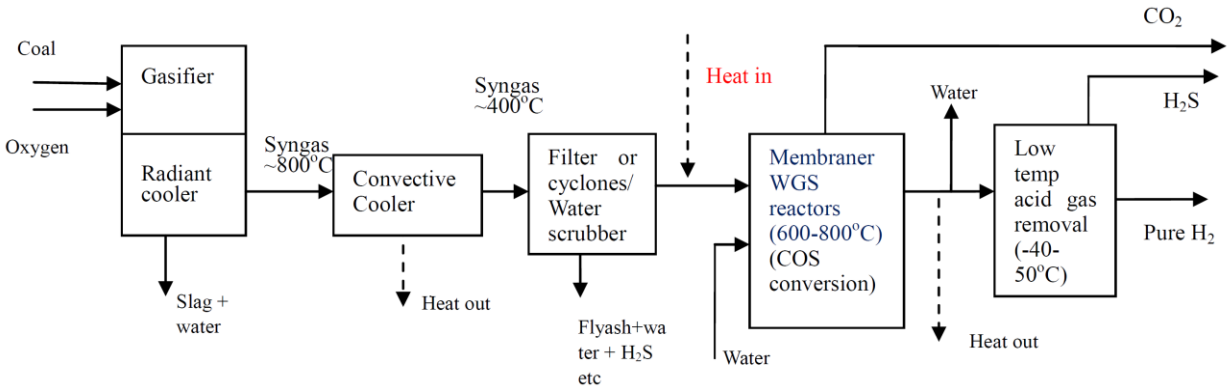

Figure 48 *Block-flow diagram of reheated ceramic-carbonate membrane reactor with CO_2 capture for IGCC power plant*

‘

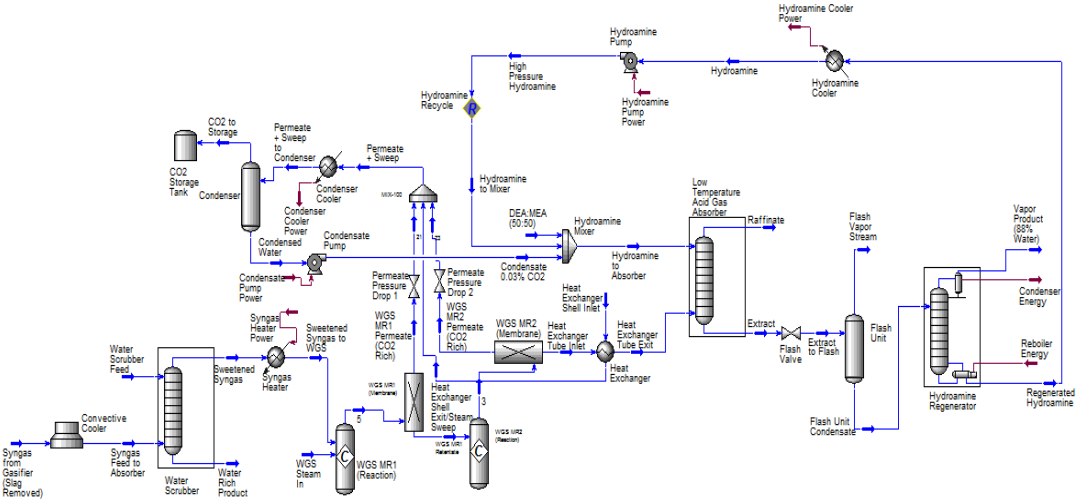

Figure 49 *Aspen HYSYS process-flow-diagram of reheated ceramic-carbonate membrane reactor with CO_2 capture for IGCC power plant*

Figures 50 and 51 show a new, high temperature ceramic-carbonate membrane WGS process with CO_2 capture. In this process, as shown in **Figure 48**, coal syngas from the gasifier is cooled down by radiant cooler to about 800-850°C, then goes through a high temperature ceramic membrane particulate separator, and a high temperature H_2S removal. The clean, hot syngas, with steam added, is fed to the new CO_2-selective ceramic-carbonate membrane reactor (without catalyst) to convert CO to H_2 and CO_2 and to separate CO_2. The gas stream from the membrane reactor (retentate stream), H_2 with a small amount of CO_2, after cooling down, is fed to a low temperature, high pressure CO_2 removal process (such as MDEA process) to produce pure H_2, and CO_2. The pure CO_2 (>99%) from the permeate stream of the membrane reactor is

cooled down and merged with the CO_2 stream from low temperature CO_2 removal unit for sequestration. This new process offers the best heat integration and offers potential savings in both equipment and operation costs. However, this integration requires development of a high temperature process for H_2S removal, and improvement of the efficiency and cost-reduction of the high temperature ceramic membrane particulate removal process.

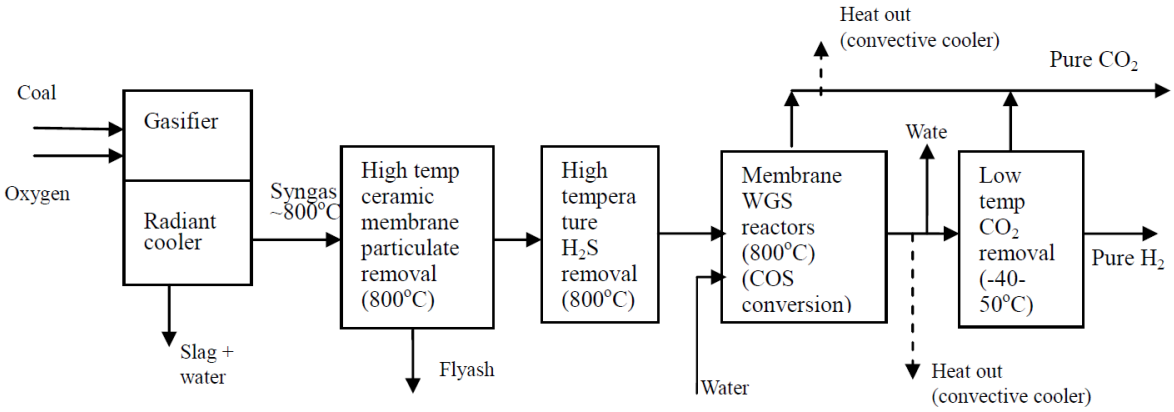

Figure 50 *Block-flow diagram of high temperature ceramic-carbonate membrane reactor with CO_2 capture for IGCC power plant*

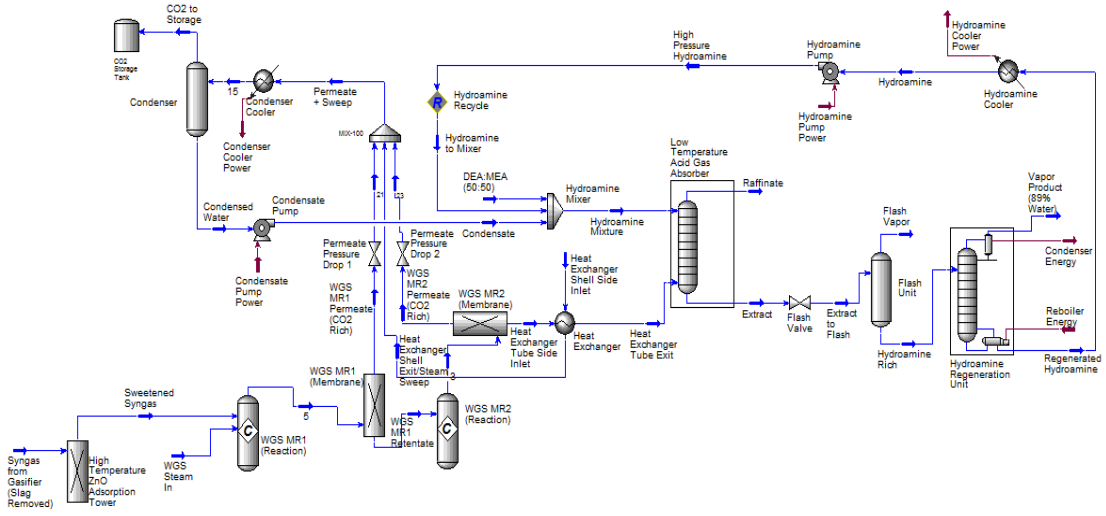

Figure 51 *Aspen HYSYS process-flow-diagram of high temperature ceramic-carbonate membrane reactor with CO_2 capture for IGCC power plant*

10.3 Cost-Estimate of WGS with CO_2 Capture by Membranes for IGCC

We have obtained mass and energy balance data for the three traditional and membrane WGS processes with CO_2 capture shown in **Figures 47, 49** and **51** for an 800 MW power plant. These data were used to estimate the capital and operation costs of the processes. **Table 12** lists production rate of syngas from gasifier for a 800 MW coal-burning IGCC power plant, rate of CO_2 capture by the membrane, membrane area and the average CO_2 through the membrane tube. From the data and assuming membrane cost of \$500/m^2, the IGCC plants with the dual-phase

membrane would need a total membrane area of about 1.7 M m^2 with a total membrane cost of about $0.86 billion. The membrane system, including required peripherals, can cost substantially more.

Table 12 *Membranes area and cost estimate for WGS with CO_2 capture by Dual-Phase Membranes*

Electric power capacity	800 MW
Coal consumption rate (mass)/s	67 kg/s
Carbon content %	60
Percentage of carbon converted to CO_2%	85
Rate of CO_2 produced	2,859 mol/s
CO_2 permeation rate (90% Capture)	2,573 mol/s
Area of membranes (2 tube in series)	600 cm^2
CO_2 flux under optimum conditions for the dual-phase membrane tested in this project	0.2 cc (STP)/cm^2.min
Estimate number of 2-tube-series	28,822,752
Total membrane area required	1,729,365 m^2
Estimate membrane costs	$864,682,560

The high cost of the membrane is due to large membrane area required because of the low flux of CO_2 (as compared to H_2 flux through Pd membranes at 400^oC). The CO_2 permeation flux listed in **Table 12** is the average value for the two-stage membrane system with target separation. Thus, to reduce the cost of the membrane reactor, one needs to significantly improve CO_2 permeance or reduce the membrane costs.

Table 13 *Rough Estimates of Major Equipment and Operation Costs for WGS with CO_2/H_2 Separation (for 800 MW Power Plant)*

WGS/Separation Processes	Equipment (excluding gasifier) (Million$)	Operation (Million $/year)
Traditional WGS with CO_2 capture, Figure 47	159	70.9
Catalyst-free membrane WGS with CO_2 capture, Figure 49	916	5.9
Catalyst-free membrane WGS with CO_2 capture, Figure 51	896	5.5

In spite of the high costs of the membranes, the membranes WGS reaction processes, **Figures 49** and **51**, provide substantial saving in the equipment costs for CO_2 separation by amine absorption due to the reduced CO_2 volume to be treated. The processes also save the costs of WGS catalyst which is not needed in the membrane reactor processes. Furthermore, operating the membrane reactor at high temperatures provide better heat-integration, reducing the operation costs. **Table 13** summarizes the estimated results of the major equipment and operation costs for the WGS reaction with CO_2/H_2 separation by traditional and membrane reactor processes described in **Figures 47, 49** and **51**. As shown in **Table 13**, the equipment

costs for the membrane WGS processes with CO2 capture are significantly higher than that of the traditional WGS process with CO_2 capture. However, the operation costs of the membrane WGS process in **Figure 49** and that in **Figure 51** are only about 8% of the traditional WGS process with CO_2 capture because the membrane processes essentially avoid energy intensive amine absorption/regeneration processes for CO_2/H_2 separation.

A 582 MW IGCC power plant with CO_2 capture by the conventional process (**Figure 47**) being built in Kemper County, Mississippi is estimated to cost $5.6 billion. If the present membrane reactor would be used in the IGCC process, the cost of the membrane system would be roughly 10-20% of the total costs of the plant, which is too high. Major efforts should be directed to improve CO_2 permeance of the dual-phase membrane by at least ten-folds so as to reduce the membrane costs. These efforts will include making the dual-phase ceramic membranes with ceramic phase of new materials with higher oxygen ionic conductivity, and reducing membrane thickness.

11. Publications on Results from this Project

The following papers have been published in referred journals reporting results obtained in this project:

1. B. Lu and Y.S. Lin, "Sol-gel synthesis and characterization of mesoporous yttria stabilized zirconia membranes with graded pore structure", *J. Materials Sci*., 46, 7056-7066 (2011)
2. M. Anderson, H.B. Wang and Y.S. Lin, "Inorganic membranes for carbon dioxide and nitrogen separation", *Review Chem. Eng*., 28, 101-121 (2012)
3. Z.B. Rui, M. Anderson , Y.D. Li, Y.S. Lin, "Ionic conducting ceramic and carbonate dual phase membranes for carbon dioxide separation", *J. Membrane Sci*., 417-418, 174-182 (2012)
4. T. T. Norton, Y.S. Lin, "Transient oxygen permeation and surface catalytic properties of lanthanum cobaltite membrane under oxygen-methane gradient", *Ind. Eng. Chem. Res*., 51, 12917-12925 (2012)
5. M. Anderson and Y.S. Lin, "Carbon dioxide separation and dry reforming of methane for synthesis of syngas by a dual-phase membrane reactor", *AIChE J*., 59, 2207-2218 (2013)
6. B. Lu, Y.S. Lin, "Synthesis and characterization of thin ceramic-carbonate dual-phase membranes for carbon dioxide separation", *J. Membr. Sci*., 444, 402-411 (2013)
7. X.L. Dong, J. Ortiz-Landeros, Y.S. Lin, "An asymmetric tubular ceramic-carbonate dual phase membrane for high temperature CO_2 separation", *Chem. Commun*, 49, 9654-9656 (2013)
8. J. Ortiz-Landeros, T. Norton and Y.S. Lin, "Effects of support pore structure on carbon dioxide permeation of ceramic-carbonate dual-phase membranes", *Chem. Eng. Sci*., 104, 891-898 (2013)
9. T.T. Norton, J. Ortiz-Landeros and Y.S. Lin, "Stability of La-Sr-Co-Fe oxide-carbonate dual-phase membranes for carbon dioxide separation at high temperatures", *Ind. Eng. Chem. Res.*, 53, 2432-2440 (2014)

10. T.T. Norton, Bo Lu and Y.S. Lin, "Carbon dioxide permeation properties and stability of samarium-doped-ceria carbonate dual-phase membranes", *J. Membr, Sci*., 467, 244-252(2014)
11. T.T. Norton and Y.S. Lin, "Ceramic-carbonate dual-phase membrane with improved chemical stability for carbon dioxide separation at high temperature", *Solid State Ionics*, 263, 172-179 (2014)
12. B. Lu, Y.S. Lin, "Asymmetric thin samarium doped cerium oxide–carbonate dual-phase membrane for carbon dioxide separation", *Ind. Eng. Chem. Res*., 53, 13459-13466 (2014)

The researchers from Arizona State University also made the following presentations on results obtained in this project:

1. B. Lu, M. Anderson, Y.S. Lin, "Synthesis and characterization of yttria-stabilized-zirconia derived supports for carbonate-ceramic dual-phase membranes", Gordon Research Conference: Membrane Materials and Processes, (Poster) New London, NH, July 25, 30, 2010
2. J. Ortiz-Landeros, M. Anderson, T. Norton, Y.S. Lin, "Effect of Ceramic/Carbonate Phase Ratio on Carbon Dioxide Permeation through Ceramic-Carbonate Dual Phase", North American Membrane Society Annual Meeting, Las Vegas, June 4-8 (2011)
3. B. Lu and Y.S. Lin, "Synthesis and Characterization of Thin Carbonate-Ceramic Dual-Phase Membranes for Carbon Dioxide Separation", North American Membrane Society Annual Meeting, Las Vegas, June 4-8 (2011) Y.S. Lin, "Ceramic-carbonate dual-phase membrane for high temperature carbon dioxide separation", Keynote lecture, *International Conference on Membrane Materials and Processes (ICOM2011)*, Amsterdam, Netherland, July 24-29, 2011
4. T. Norton, J. Ortiz-Landeros, Y.S Lin, "Ceramic-carbonate dual-phase membrane for high temperature carbon dioxide separation from nitrogen", North American Membrane Society Annual Meeting, New Orleans, LA, June 9-13 (2012)
5. B. Lu, Y.S. Lin, "Synthesis and characterization of thin samarium doped ceria/ carbonate dual-phase membranes for high temperature carbon dioxide separation", North American Membrane Society Annual Meeting, Boise, ID, June 8-12, (2013)
6. T. Norton, J. Ortiz-Landeros, Y.S. Lin, "Ceramic-carbonate dual-phase membrane for high temperature carbon dioxide separation ", North American Membrane Society Annual Meeting, Boise, ID, June 8-12, (2013)
7. B. Lu, Y.S. Lin, "Synthesis and characterization of thin samarium doped ceria/ carbonate dual-phase membranes for high temperature carbon dioxide separation", North American Membrane Society Annual Meeting, Boise, ID, June 8-12, (2013)
8. T. Norton, J. Ortiz-Landeros, Y.S. Lin, "Ceramic-carbonate dual-phase membrane for high temperature carbon dioxide separation ", North American Membrane Society Annual Meeting, Boise, ID, June 8-12, (2013)
9. Y.S. Lin, "High Temperature Inorganic Membranes for Hydrogen or Carbon Dioxide Separation", Dept. Earth and Environmental Engineering, Columbia University, New York, NY, October 26, 2012
10. Y.S. Lin, "Synthesis of dual-phase membranes for carbon dioxide capture", China Electrical Power Research Institute, Beijing, Aug.14, 2013

11. Y.S. Lin, "Dual-phase membranes for carbon dioxide capture", Dept. of Chemical and Biological Engineering, University of South Carolina, Columbia, SC, Oct.23, 2013
12. Y.S. Lin, "High temperature membranes for carbon dioxide capture", Nanoscale Science Seminar, Dept. of Phys., Arizona State University, Tempe, AZ, Feb.10, 2014
13. Y.S. Lin, "Dual-phase ceramic-carbonate membranes for CO_2 separation", Dept. of Chemical and Biological Engineering, Colorado School of Mines, Golden, CO, April 25, 2014
14. Y.S. Lin, Carbon Dioxide Perm-Selective Ceramic-Carbonate Dual-Phase Membranes, Plenary Lecture, 13th International Conference on Inorganic Membranes (ICIM2014), Brisbane, Australia, July 6-9, 2014
15. Y.S. Lin, Ceramic-Carbonate Membrane Reactors for Chemical Reactions with Carbon Dioxide Separation, Keynote Lecture, 10th International Congress on Membranes and Membrane Processes (ICOM2014), Suzhou, China, July 20-25, 2014

12. Conclusions

A series of CO_2 perm-selective disk and tubular ceramic-carbonate membranes with the thickness of 10 μm to 1.5 mm were fabricated. CO_2 permeance of these membranes are in the range of 0.5-5 $\times 10^{-7}$ mol m^{-2} s^{-1} Pa^{-1} at 500-900 ^oC. These membranes show extremely high CO_2 perm-selectivity (up to 3000) and high stability for high temperature CO_2 separation.

CO_2 permeation flux was mainly controlled by the ionic conductivity of the ceramic phase and also affected by other factors, such as temperature, CO_2 partial pressure across the membrane, membrane thickness and membrane microstructure. A reliable CO_2 permeation model was developed. A theoretical method was established for the optimization of the microstructures of ceramic-carbonate membranes.

Both modeling and experimental studies confirmed that high temperature syngas WGS reaction in tubular SDC-carbonate dual phase membrane reactor was feasible even without catalyst. It is possible to produce hydrogen of 93% purity and CO_2 stream of >95% purity with 90% CO_2 capture under optimized conditions.

The integration of the ceramic-carbonate dual-phase membrane reactor with IGCC process for carbon dioxide capture was analyzed by a model for membrane reactor, and HYSYS process design and analysis. The calculation results showed that dual-phase membrane reactor could improve IGCC process efficiency but the membrane reactor is too expensive with the dual-phase membranes having current CO_2 permeance obtained in this project. However, future efforts to making dual-phase membranes with higher CO_2 permeance would reduce the membrane costs, which, combined with substantial reduction in operation costs, would make the membrane reactor an attractive option to be integrated into IGCC with CO_2 capture.

13. References Cited

[1] T.F. Wall, Combustion Processes for carbon capture, Proceedings of the Combustion Institute, 31, 31 (2007).
[2] C. Ratnasamy, J. Wagner, Water gas shift catalysis, Catal. Rev. 51 (2009) 325–440.
[3] S. Smart, C.X.C. Lin, L. Ding, K. Thambimuthub, J.C.D. da Costa, Ceramic membranes for gas processing in coal gasification, Energy Environ. Sci. 3 (2010) 268–278.

[4] K. Babita, S. Sridhar, K.V. Raghavan, Membrane reactors for fuel cell quality hydrogen through WGSR–review of their status, challenges and opportunities, Int. J. Hydrogen Energy 36 (2011) 6671–6688.
[5] F. Gallucci, E. Fernandez, P. Corengia, M.S. Annaland, Recent advances on membranes and membrane reactors for hydrogen production, Chem. Eng. Sci. 92 (2013) 40–66.
[6] Y.D. Bi, H.Y. Xu, W.Z. Li, A. Goldbach, Water–gas shift reaction in a Pd membrane reactor over $Pt/Ce_{0.6}Zr_{0.4}O_2$ catalyst, Int. J. Hydrogen Energy 34 (2009) 2965–2971.
[7] S.H. Lee, J.N. Kim, W.H. Eomb, S.K. Ryi, J.S. Park, H. Baek Il, Development of pilot WGS/multi-layer membrane for CO_2 capture, Chem. Eng. J. 207–208 (2012) 521–525.
[8] J. Catalano, F. Guazzone, I.P. Mardilovich, N.K. Kazantzis, Y.H. Ma, Hydrogen production in a large scale water gas shift Pd-based catalytic membrane reactor, Ind. Eng. Chem. Res. 52 (2013) 1042–1055.
[9] A.S. Damle, S.K. Gangwal, V.K. Venkataraman, A simple-model for a water-gas shift membrane reactor, Gas Sep. Purif. 8 (1994) 101–106.
[10] M. Bracht, P.R Alderliesten, R. Kloster, R. Pruschek, G. Haupt, E. Xue, J.R. H. Ross, M.K. Koukou, N. Papayannakos, Water gas shift membrane reactor for CO_2 control in IGCC systems: Techno-economic feasibility study, Eng. Conv. Manag. 38 (1997) S159–S164.
[11] Criscuoli, A. Basile, E. Drioli, O, Loiacono, An economic feasibility study for water gas shift membrane reactor, J. Membr. Sci. 181 (2000) 21–27.
[12] V. Francuz, Modeling of Membrane Reactor for Water-Gas-Shift Reaction, Internal Report for Carbon Dioxide Project (2002).
[13] M.B. Shiflett, H.C. Foley, Ultrasonic deposition of high-selectivity nanoporous carbon membranes, Science, 285 (1999) 1902–1905.
[14] C.W. Jones, W.J. Koros, Characterization of ultramicroporous carbon membranes with humidified feeds, Ind. Eng. Chem. Res. 34 (1995) 158–163.
[15] A. Brunettia, G. Barbieria, E. Driolia, T. Granatob, K.H. Lee, A porous stainless steel supported silica membrane for WGS reaction in a catalytic membrane reactor, Chem. Eng. Sci. 62 (2007) 5621–5626.
[16] S. Battersby, M.C. Duke, S.M. Liu, V. Rudolph, J.C.D. da Costa, Metal doped silica membrane reactor: operational effects of reaction and permeation for the water gas shift reaction, J. Membr. Sci. 316 (2008) 46–52.
[17] S.J. Kim, Z. Xu, G.K. Reddy, P. Smirniotis, J.H. Dong, Effect of pressure on high-temperature water gas shift reaction in microporous zeolite membrane reactor, Ind. Eng. Chem. Res. 51 (2012) 1364–1375.
[18] H.B. Wang, X.L. Dong, Y.S. Lin, Highly stable bilayer MFI zeolite membranes for high temperature hydrogen separation, J. Membr. Sci. 450 (2014) 425–432.
[19] P.S. Maiya, T.J. Anderson, R.L. Mieville, J.T. Dusek, J.J. Picciolo, U. Balachandran, Maximizing H_2 production by combined partial oxidation of CH_4 and water gas shift reaction, Appl. Catal. A: Gen.196 (2000) 65–72.
[20] J. Li, H.Yoon, T.K. Oh, E.D. Wachsman, Stability of $SrCe_{1-x}Zr_xO_{3-\delta}$ under water gas shift reaction conditions, J. Electrochem. Soc. 157 (2010) B383–B387.
[21] Y.S. Lin, I. Kumakiri, B.N. Nair, H. Alsyouri, Microporous inorganic membranes, Sep. Purif. Methods 32 (2002) 229–379.
[22] M.C. Duke, J.C.D. da Costa, D.D. Do, P.G. Gray, G.Q. Lu, Hydrothermally robust molecular sieve silica for wet gas separation, Adv. Funct. Mater. 16 (2006) 1215–1220.

[23] H. Iwahara, Proton conducting ceramics and their applications, Solid State Ionics, 86–88 (1996) 9–15.
[24] A. Kulprathipanja, G.O. Alptekin, J.L. Falconer, J.D. Way, Effects of water gas shift gases on Pd−Cu alloy membrane surface morphology and separation properties, Ind. Eng. Chem. Res. 43 (2004) 4188–4198.
[25] O. Iyoha, B. Howard, B. Morreale, R. Killmeyer, R. Enick, The effects of H_2O, CO and CO_2 on the H_2 permeance and surface characteristics of 1 mm thick $Pd_{80wt\%}Cu$ membranes, Top. Catal. 49 (2008) 97–107.
[26] M. Kanezashi, J. O'Brien-Abraham, Y.S. Lin, K. Suzuki, Gas permeation through DDR-type zeolite membranes at high temperatures, AIChE J. 54 (2008) 1478–1486.
[27] H. M. Jang, K. B. Lee, H. S. Caram, S. Sircar, High-purity hydrogen production through sorption enhanced water gas shift reaction using K_2CO_3-promoted hydrotalcite, Chem. Eng. Sci. 73 (2012) 431–438.
[28] M. S. Duyar, R. J. Farrauto, M. J. Castaldi, T. M. Yegulalp, In situ CO_2 capture using CaO/γ-Al_2O_3 washcoated monoliths for sorption enhanced water gas shift reaction, Ind. Eng. Chem. Res. 53 (2014) 1064−1072.
[29] C. A. Scholes, K. H. Smith, S. E. Kentish, G. W. Stevens, CO_2 capture from pre-combustion processes—Strategies for membrane gas separation, Int. J. Green. Gas Control 4 (20100) 739–755.
[30] M. Anderson, H. B. Wang, Y. S. Lin, Inorganic membranes for carbon dioxide and nitrogen separation, Rev. Chem. Eng. 28 (2012) 101–121.
[31] Y. Sakamoto, K. Nagata, K. Yogo, K. Yamada, CO_2 separation properties of amine-modified mesoporous silica membranes, Micropor. Mesopor. Mater. 101 (2007) 303–311.
[32] S. Li, C.Q. Fan, High-Flux SAPO-34 Membrane for CO_2/N_2 Separation, Ind. Eng. Chem. Res. 49 (2010) 4399–4404.
[33] S. J. Chung, J. H. Park, D. Li, J.-I. Ida, I. Kumakiri, J. Y. S. Lin, Dual-phase metal−carbonate membrane for high-temperature carbon dioxide separation, Ind. Eng. Chem. Res. 44 (2005) 7999–8006.
[34] M. Anderson, Y.S. Lin, Carbonate–ceramic dual-phase membrane for carbon dioxide separation, J. Membr. Sci. 357 (2010) 122–129. (Change to ICIM proceeding)
[35] Q. Yin, Y.S. Lin, Beneficial effect of order–disorder phase transition on oxygen sorption properties of perovskite-type oxides, Solid State Ionics, 178 (2007) 83–89.
[36] B. Lu, Y.S.Lin, Synthesis and characterization of thin ceramic-carbonate dual-phase membranes for carbon dioxide separation, J. Membr. Sci. 444 (2013) 402–411.
[37] B. Lu, Y.S. Lin, Asymmetric thin samarium doped cerium oxide–carbonate dual-phase membrane for carbon dioxide separation, Ind. Eng. Chem. Res. 53 (2014) 13459–13466.
[38] Z.B Rui, M. Anderson, Y.D. Li, Y.S. Lin, Ionic conducting ceramic and carbonate dual phase membranes for carbon dioxide separation, J. Membr. Sci. 417–418 (2012) 174–182.
[39] T.T. Norton, Y.S. Lin, Ceramic-carbonate dual-phase membrane with improved chemical stability for carbon dioxide separation at high temperature, Solid State Ionics, 263 (2014) 172–179.
[40] T.T. Norton, B. Lu, Y.S. Lin, Carbon dioxide permeation properties and stability of samarium-doped-ceria carbonate dual-phase membranes, J. Membr. Sci. 467 (2014) 244–252.
[41] Z.B. Rui, M. Anderson, Y.S. Lin, Y.D. Li, Modeling and analysis of carbon dioxide permeation through ceramic-carbonate dual-phase membranes, J. Membr. Sci. 345 (2009) 110–118.

[42] J. Ortiz-Landeros, T. Norton, Y.S. Lin, Effects of support pore structure on carbon dioxide permeation of ceramic-carbonate dual-phase membranes, Chem. Eng. Sci. 104 (2013) 891–898.
[43] H.J.M. Bouwmeester, A.J. Burggraaf, Dense ceramic membranes for oxygen separation, in "Fundamentals of inorganic membrane science and technology", Eds A.J. Burggraaf, L. Cot, Chapter 10, Elsevier (1996).
[44] Z. Yang, Y.S. Lin, Equilibrium of oxygen sorption on perovskite type ceramic sorbents, AIChE J. 49 (2003) 793–798.
[45] X.L. Dong, J. Ortiz-Landeros, Y.S. Lin, Asymmetric tubular ceramic-carbonate dual phase membrane for high temperature CO_2 separation, Chem. Comm. 49 (2013) 9654–9656.
[46] L. Zhang, N. Xu, X. Li, S. Wang, K. Huang, W. H. Harris, W.K.S. Chiu, High CO_2 permeation flux enabled by highly interconnected three-dimensional ionic channels in selective CO_2 separation membranes, Energy Environ. Sci. 5 (2012) 8310–8317.
[47] X. Li, G. Xiao, K. Huang, Effective ionic conductivity of a novel intermediate-temperature mixed oxide-ion and carbonate-ion conductor, J. Electrochem. Soc. 158 (2011) B225–232.
[48] G.K. Reddy, K. Gunasekera, P. Boolchand, J. Dong, P.G. Smirniotis, High Temperature Water Gas Shift Reaction over Nanocrystalline Copper Codoped-Modified Ferrites, J. Phys. Chem. C 115 (2011) 7586–7595.
[49] T. Mori, Y. Wang, J. Drennan, G. Auchterlonie, J. G. Li and T. Ikegami, Influence of particle morphology on nanostructural feature and conducting property in Sm-doped CeO_2 sintered body, Solid State Ionics 175 (2004) 641–649.
[50] M. V. Ciocco, B. D. Morreale, K. S. Rothenberger, B. H. Howard, R. P. Killmeyer, R. M. Enick and F. Bustamante, Water-gas shift membrane reactor studies, NETL Report, 2005.
[51] F. Bustamante, R. M. Enick, R. P. Killmeyer, B. H. Howard, K. S. Rothenberger, A. V. Cugini, B. D. Morreale, M. V. Ciocco, Uncatalyzed and wall-catalyzed forward water–gas shift reaction kinetics, AIChE J. 51 (2005) 1440–1454.
[52] O. Iyoha, H_2 production in palladium & palladium-copper membrane reactors at 1173K in the presence of H_2S, PhD thesis, University of Pittsburgh, (2007).
[53] O. Iyoha, R. Enick, R. Killmeyer, B. Howard, M. Ciocco, B. Morreale, H_2 production from simulated coal syngas containing H_2S in multi-tubular Pd and 80 wt% Pd–20 wt% Cu membrane reactors at 1173 K, J. Membr. Sci. 306 (2007) 103–115.